Biomath Communications

https://biomath.math.bas.bg/biomath/index.php/conference

Multiphysics Simulations of the Process of Neuromuscular Activation

Zdravka Ivanova

Faculty of Mathematics and Informatics,
Sofia University "St. Kliment Ohridski", Bulgaria
zivanova@fmi.uni-sofia.bg

Abstract

In this Master's thesis, we consider the problem of mathematical modelling and computer simulations of neuromuscular activation. We describe the biological and biochemical processes that result in a muscle contraction. For each of them, we derive a mathematical model, established in the literature. In particular, we consider:

- the Hodgkin–Huxley model of neural transmission;
- a reaction-diffusion model for the process of neurotransmitter release in the synaptic gap between a nerve and a muscle cell;
- an ODE system, based on chemical reaction schemes, proposed by Williams, for the process of calcium dynamics inside the muscle cell;
- Hill's model for the generation of muscle force, triggered by calcium dynamics.

We study the models numerically to illustrate the behaviour of the model solutions and to interpret them from a biological point of view. For the model of calcium dynamics, we also make qualitative analysis and obtain original results for the asymptotic behaviour of the model solutions.

Further, we propose a framework for coupling the models, mentioned above, so that we can obtain new integrated multiphysics simulations of the whole process.

Our initial motivation for the study is the future application of the proposed approach for modelling neuromuscular diseases. Therefore, the framework we propose is based on the idea of modelling micro-scale processes and studying their effect on the macro-scale muscle action.

Received: September 28, 2022, Accepted: December 12, 2022, Published: February 10, 2023
Citation: Zdravka Ivanova, Multiphysics Simulations of the Process of Neuromuscular Activation, Biomath Communications 9 (2022), 2212129,
https://doi.org/10.55630/bmc.2022.12.129

Contents

1 Introduction

Neuromuscular disease is a broad term that is connected with a malfunctioning of the neuromuscular system that can affect any part of a nerve or a muscle. Nowadays, most of the neuromuscular diseases are still incurable, despite the quick development in all areas of human society, including medicine. An example list of neuromuscular diseases is shown in Fig. 1.

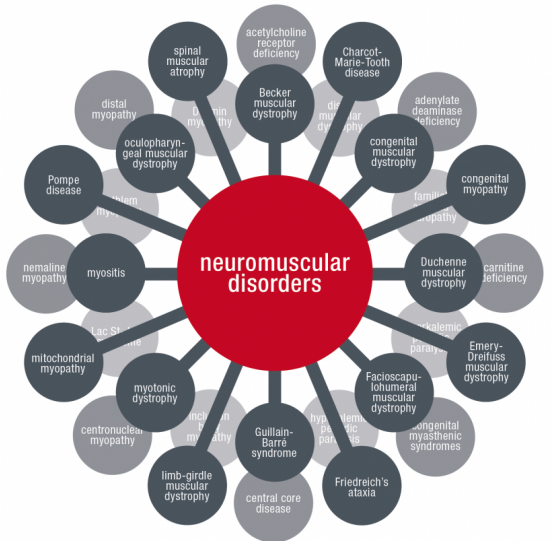

Figure 1: A diagram of some of the neuromuscular diseases [1].

The neuromuscular system combines the nervous system and muscles to work together and permit movement. Neuromuscular diseases are diseases that affect the normal functioning of the muscles and/or their control from the nervous system. Such diseases are caused by autoimmune or genetic disorders as well as contact with environmental chemical substances or other influences [2]. Therefore, to model such a disease one should apply a detailed integrated approach—modelling of the nervous system, the resulting muscle activity and the connection between them. The process of muscle contraction can be modeled as the result of four different consecutive processes—propagation of nerve impulse, neurotransmitter release in the space between the nerve and the muscle, the resulting biochemical reactions in the muscle, and the generated contraction.

In this thesis, we shall give a detailed description of the process of muscle activation and shall propose an integrated mathematical model for the whole process. Our aim is to lay the foundations for studying the mechanisms of different neuromuscular diseases in the future.

1.1 The main biological structures in the process

Here, we give a brief information about the structure of a skeletal muscle and a nerve cell—the two main biological structures that will be of interest for our further studies.

1.1.1 Skeletal muscle morphology

A general cross-section of a skeletal muscle [3] can be seen in Fig. 2.

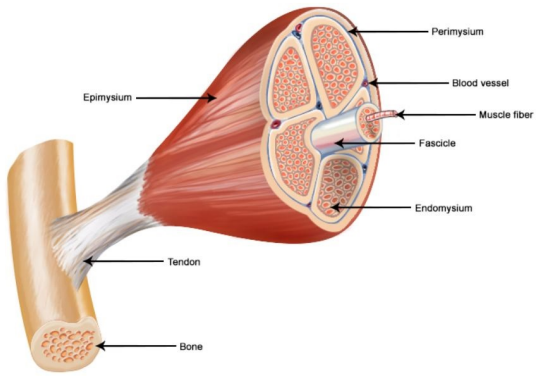

Figure 2: Skeletal muscle morphology [4].

The hierarchical structure in the skeletal muscle is described as follows:

- A skeletal muscle is surrounded by fibrous tissue, called *epimysium*. It serves as a protection shield and protects the muscle from friction against other muscles and bones;
- Within the muscle, there is another connective tissue, the *perimysium*, which connects muscle fibers into bundles, called fascicles. A large muscle contains more fibers in each bundle, while a small one contains less;
- Inside the fascicles there is another connective tissue, which isolates each fiber, called *endomysium*;
- The endomysium contains the muscle cells/fibers or *myofibers*, formed in the process of myogenesis. Every myofiber can have a different length up to several centimeters, which is the reason that the muscle cells have multiple nuclei.

In Fig. 3, the structure of a muscle fiber is shown. The membrane of the muscle cell, called sarcolemma, contains a bunch of tubes called myofibrils—the

contractile units of the cell. Each muscle fiber contains hundreds or thousands of myofibrils, which are divided into segments called sarcomeres. The sarcomeres are the basis for muscle contraction theory, known as the sliding filament theory.

Each sarcomere is separated by a border, called a *Z-line* or a *Z-disc*. As in Fig. 3, the sarcomere is composed of long fibrous proteins. It contains two main types of long protein chains, called **filaments**[1]—thin, made of actin protein strands and thick—composed of myosin protein strands. Muscle contraction happens, because of thin and thick filaments sliding past each other through complex biochemical processes, triggered by calcium dynamics inside the muscle cell.

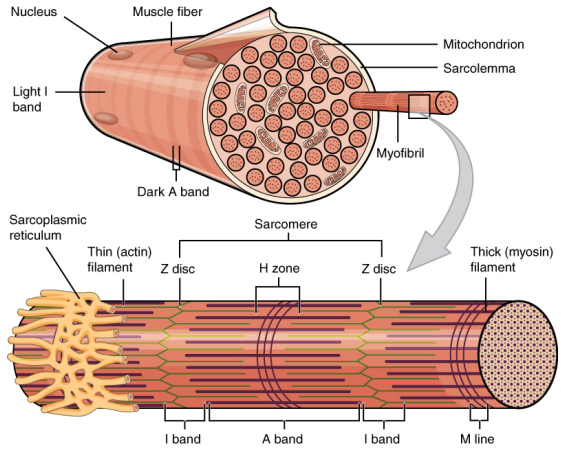

Figure 3: A muscle fiber structure [5].

Each muscle cell has the so-called **sarcoplasmic reticulum** (SR), which is a membrane-bound network of tubules that wraps the myofibrils. **The main function of the SR is to store calcium ions.**

1.1.2 The structure of a nerve cell

A typical neuron consists of the following main parts [6], see Fig. 4:

- dendritic trees—structures in the neuron that receive and process electrical messages; a single neuron may have more than one set of dendrites and may receive thousands of input signals;

[1] We have marked in bold the crucial terms related to the muscle structure that will be used throughout the MSc thesis.

- cell body (soma)—a part of the neuron that contains the nucleus. It connects to the dendrites and the axon via which the neuron sends information to other neurons;
- axon—a long projection that is responsible for carrying electrical impulses away from the cell body;
- axon terminal (axonal tree)—the end of the axon, which has a tree-like structure and contains synapses, see Fig. 5, which are responsible for the injection of pulses of ionic current (or electric charge) into the dendrites and cell body of other cells in response to signals.

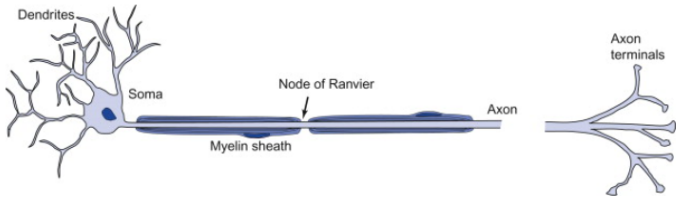

Figure 4: Structure of a motor neuron [7].

Most motor neurons (as well as many other nerve cells) have the so-called myelin sheath, a lipid-rich substance, which isolates the axon and helps it to increase the speed at which information (an electrical signal) travels. Myelin sheath does not cover the axon entirely, but is disrupted at gaps, called nodes of Ranvier.

When a neuron passes a signal to another neuron or a muscle cell, it transmits a chemical messenger, called neurotransmitter, that is released from synaptic vesicles in the synapses of the axonal tree through the synaptic cleft, see Fig. 5.

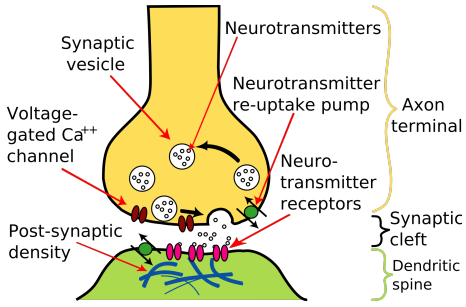

Figure 5: Structure of a typical chemical synapse [8].

1.2 The process of muscle activation

To model the process of muscle activity, we shall consider the scheme, presented in Fig. 6, which gives a possible description of the whole process. We shall describe the different steps here and shall elaborate further in the corresponding sections later on.

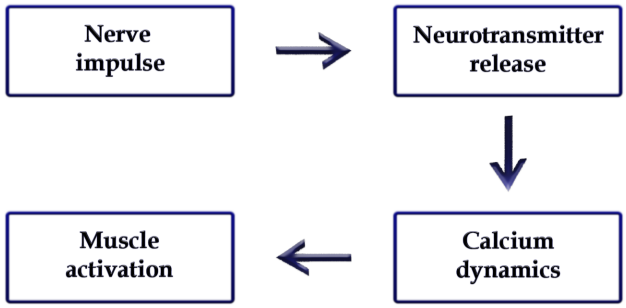

Figure 6: The process of muscle activation.

Nerve impulses, also known as action potentials, are electric signals that travel from the brain or the spinal cord along the long axons of the motor neurons to the axon terminals, where the impulses are transferred to the so-called motor end plate of a skeletal muscle fiber, see Fig. 7. The gap between the axon of a motor neuron and a motor end plate, where the impulses are transmitted, is called a neuromuscular junction. The process that leads to a contraction of a

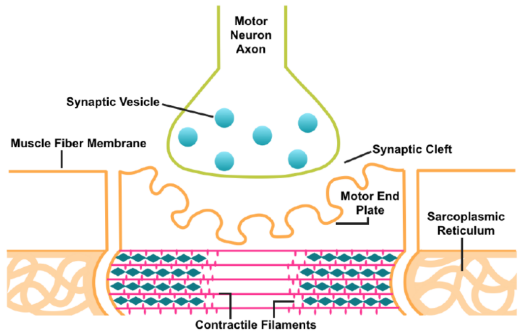

Figure 7: The neuromuscular junction [9].

muscle fiber and its connection with the activity of motor neurons is illustrated in Fig. 8 and can be described in the following steps [10]:

1. An impulse travels through the axon of the motor neuron to the axon terminal;

2. At the axon terminal there are voltage-gated calcium channels, which open due to the action potential and calcium ions diffuse into the terminal;

3. The calcium presence in the axon terminal opens the so-called synaptic vesicles to release a neurotransmitter, called acetylcholine (ACh);

4. The released ACh diffuses, crosses the synaptic cleft and binds to ACh receptors on the motor end plate of the muscle, which contains cation channels. The cation channels open and sodium ions enter the muscle fiber, causing potassium ions to exit the muscle fiber;

5. The input flux of the sodium ions changes the membrane potential, causing depolarization or the so-called end plate potential (EPP). Once the membrane potential reaches a threshold value, an action potential propagates along the sarcolemma;

6. Inside the muscle cell, the sarcoplasmic reticulum (SR), which is a network of tubules that regulates calcium concentration, then releases calcium so that it can bind to contractile filaments (CFs) in the muscle fiber. The binding of calcium to the CFs (actin and myosin filaments) allows them to bind to each other and further leads to muscle cell contraction.

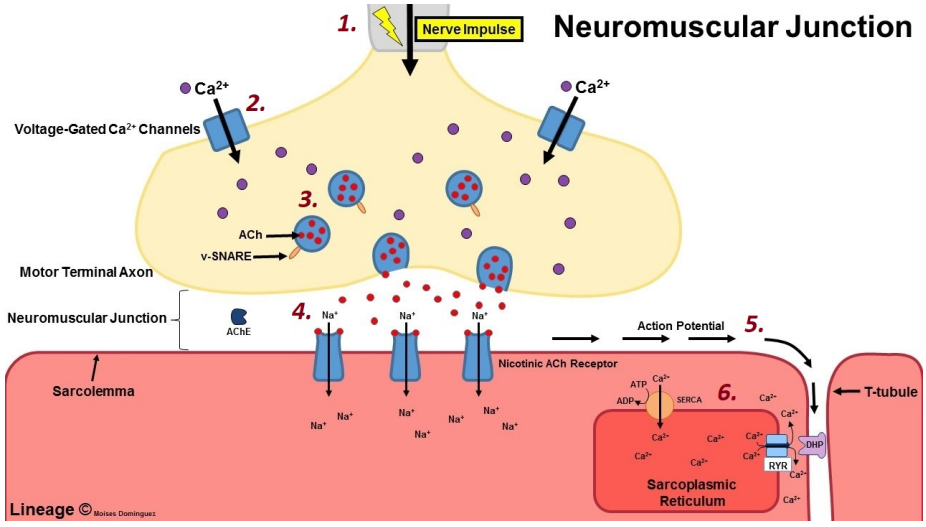

Figure 8: The process of a muscle contraction in steps (1)–(6) [11].

The sliding filament theory, invented separately by two research teams in the 20th century [12], describes the process of muscle contraction based on the thin and thick filaments that slide past each other to generate movement, triggered by the calcium dynamics inside the muscle cell. The process of muscle contraction is described in Fig. 9 and can be generalized in the following steps [9]:

- At rest, the myosin molecules inside the thick filaments have adenosine diphosphate molecules (ADP) and inorganic phosphate molecules (IP), attached to the individual myosin heads, while the thin filaments contain actin and different receptors (tropomyosin and troponin). When we move, the brain sends signals to the muscle cells, which as we discussed causes calcium to be released from the sarcoplasmic reticulum. Ca^{2+} ions bind to the receptors on the actin (thin filaments), which causes the latter to change shape. Thus, free space is revealed for the myosin to attach. This is called a *cross-bridge*;
- After the attachment, the ADP and IP leave the myosin, causing it to contract, and pull the actin towards it;
- The ADP and IP then combine and form ATP molecules, which again bind to the myosin and pull it away from the actin;
- After that, the ATP converts back to ADP and IP and the process repeats.

1.3 Goals and structure of the MSc thesis

The main goals of the present MSc thesis are the following:

- To give an overview of the process of neuromuscular activation, allowing its deconstruction into different subprocesses that can be modelled individually (see Fig. 6);
- To identify possible mathematical models (described usually by nonlinear systems of ordinary and/or partial differential equations) for each part of the proposed framework;
- To propose effective numerical schemes for solving the chosen mathematical models;
- To carry out numerical experiments and/or study the models analytically in order to improve our intuition about the considered biological and biochemical processes;
- To propose a new mathematical model, which couples the considered differential problems into an integrated multiphysics model of the whole process of muscle activation.

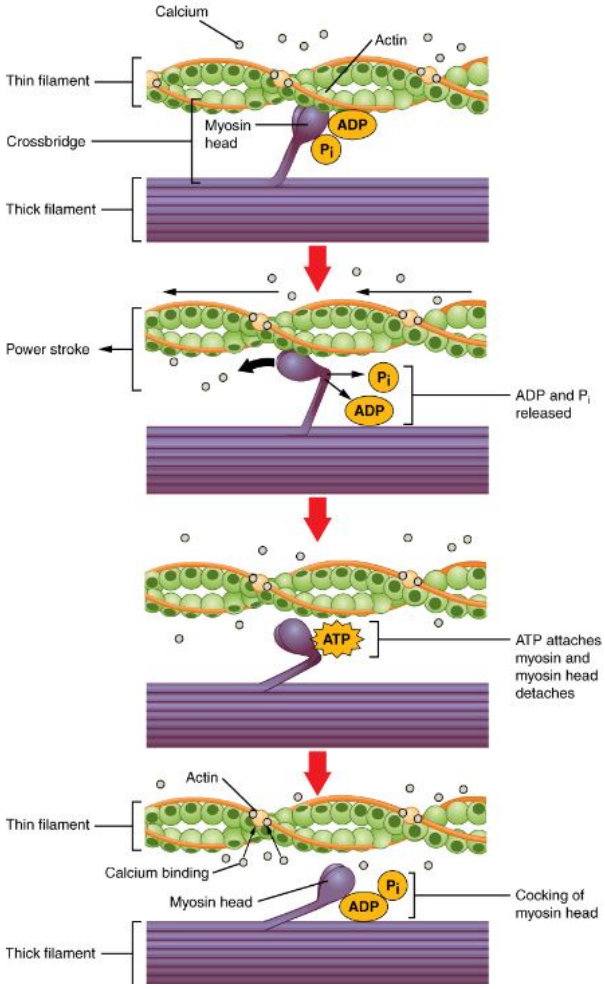

Figure 9: The sliding filament theory [5].

The MSc thesis is structured as follows:

- In Section 2, we describe the process of nerve impulse propagation and derive the classical Hodgkin–Huxley model for unmyelinated axons (described by a system of four PDEs) as well as its modification for myelinated ones (which comprises of a system of differential-difference equations). Then, we construct numerical schemes for both models and carry out numerical simulations of nerve impulse propagation;
- In Section 3, we consider a mathematical model, based on the mass action

law, for the process of calcium dynamics inside the muscle cell, which is described by a system of two ODEs. We obtain original results for the qualitative behaviour of the system, which we illustrate with phase portraits, and make corresponding observations from a biological point of view. Numerical results are presented for biologically relevant parameter values, known in the literature;

- The next Section 4 presents the two approaches that we propose for coupling the process of nerve impulse propagation and calcium dynamics. The first approach assumes a direct relation between the nerve impulse and the resulting chemical reactions in the muscle cell, while the second approach considers a 1D reaction-diffusion model for neurotransmitter release in the neuromuscular junction. To the best of our knowledge, the particular integrated model, obtained in this way, has not been described in the scientific literature;
- Section 5 gives a quick idea about the modelling of the force generation in the muscle. To this end, we couple the calcium dynamics with the classical Hill's model;
- Some additional information about the derivation of the Hodgkin–Huxley model and their experiments as well as some basic notions from the qualitative theory of dynamical systems are given in the Appendix.

2 Modelling of nerve impulses

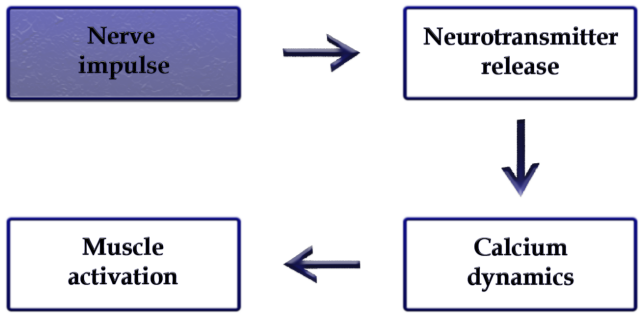

In this section, we shall discuss the process of nerve impulse transmission and shall use the classical model of Hodgkin–Huxley [13] to model it in the case of an unmyelinated axon. Further, following the pure saltatory theory [14], we reformulate the model for the case of a myelinated axon. Numerical results for known parameters from the literature are presented in both situations.

2.1 Biological preliminaries

We described the general structure of a nerve cell in Section 1.1.2. Now, we shall discuss the process of nerve impulse transmission. Since the latter is basically electric current, flowing down the axon, we need to discuss the electrical properties of the nerve cell. In particular, we shall describe the membrane structure, which is essential for the process [13].

2.1.1 Neuron membrane

The cell body and the axon of a neuron are covered by a membrane that is a bilayer of lipid molecules containing many types of protein structures. These molecules have a hydrophilic (which stands for water-loving), or polar heads, and a hydrophobic ("water-fearing"), or non-polar tails, see Fig. 10. The essential property of this bilayer is that it serves as an electric insulator. When

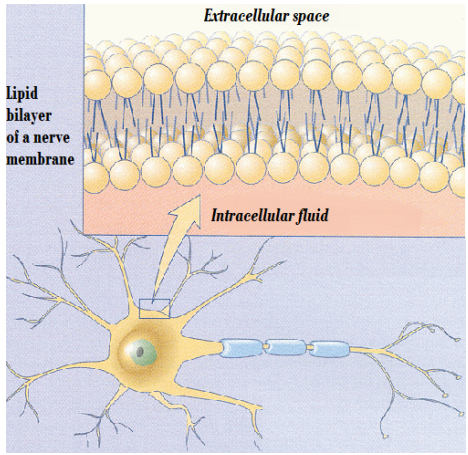

Figure 10: The nerve membrane is mainly constructed of a lipid bilayer [15].

a neuron is at its resting state, there is a potential difference, called a **resting potential**, between the inside and outside of the membrane. On both sides of the membrane, there are unequally distributed variously charged ions, mainly K^+, Na^+ and Cl^-. This leads to a potential difference, which is measured to be around -70 mV at resting state. Let us point out the following:

- at resting state, the concentration of sodium ions is higher outside the cell;
- at resting state, the concentration of potassium ions is higher inside the cell.

Among the molecules of the lipid bilayer there are also ion channels—large proteins that provide passage across the membrane, see Fig. 11.

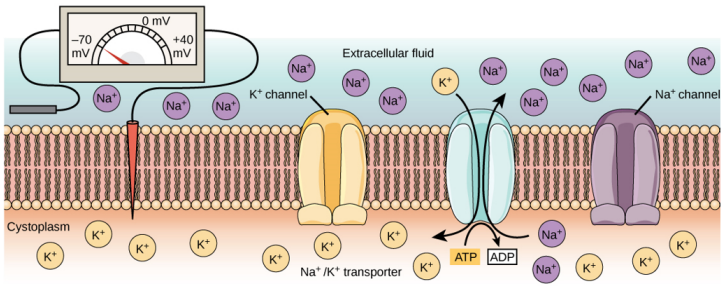

Figure 11: Neural membrane at rest [16].

These proteins are divided in the following groups [17]:

(i) passive/leakage ion channels—they are always open and are located on the dendrites, cell body, and axon;

(ii) chemically-gated ion channels—proteins, which open to allow ions such as Na^+, K^+, Ca^{2+}, or Cl^- to cross the neural membrane in response to the binding of a chemical messenger, i.e., a neurotransmitter;

(iii) voltage-gated ion channels—proteins, located on the axon and at the synapses, which form ion channels that are activated by changes in the electrical membrane potential near the channel.

All of the ion channels are selective—they allow only a certain type and amount of ions to cross, depending on the charge and size of the ion, and prevent the passage of the others.

Capacitive properties of the membrane

Because of the difference between the electric charges inside and outside the neuron, the membrane has a very important electrical property. It serves as an insulator in a capacitor.

Capacitor [18] is a charge-storing component in an electric chain, consisting of two conductors that have opposite charges and are separated by a dielectric (insulator), see Fig. 12. The charge difference creates an electric field between the plates of the capacitor.

The charge Q, stored in the capacitor, is proportional to the voltage V, i.e.,

$$Q = cV, \tag{1}$$

where c is called capacitance [19].

From what we said above, it is evident that the lipid bilayer has the property of a capacitor. It does not allow ions to cross and its hydrophilic heads "play the role" of the plates in the capacitor.

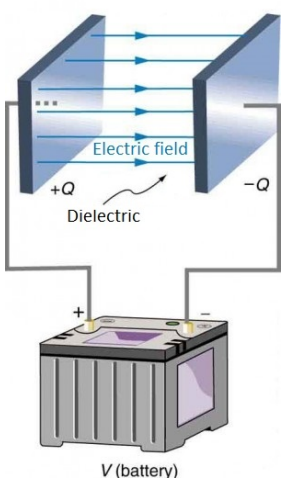

Figure 12: A capacitor [20].

2.1.2 Nerve impulse transmission

The nerve impulses are transmitted as a domino effect. Each neuron gets an impulse and passes it to the next one. When there is a signal, a neuron receives information by its dendrites and transmits it using its axonal tree. The process of impulse transmission in a neuron down its axon can be described in the following steps:

- Resting potential
  When a neuron is at rest, more Na^+ ions are located outside and more K^+ ions are located inside its axon. The difference of the electrical potentials across its membrane is called the resting membrane potential or the resting potential. In this state, the membrane is said to be **polarized**. The polarization of the neuron means that the electrical charge in its internal environment is negative with respect to the outside.

- Action potential
  When a nerve cell receives a sufficiently strong signal, a so-called action potential is triggered. It consists of the following steps, depicted in Fig. 13:

  - Voltage-gated sodium ion channels in the axon membrane open and allow Na^+ to flow through the membrane and inside the axon. This leads to an increase in the membrane potential, called **depolarization**;

- On the following steps, voltage-gated potassium ion channels open, which allows the potassium to flow out of the neuron, and sodium channels close;
- When no more sodium ions can enter the cell, the voltage decreases, which is known as **repolarization**;
- Next, the potassium channels close. At this point, the voltage is below the resting potential, which is known as **hyperpolarization**;
- Finally, the potential rises again and reaches the resting potential.

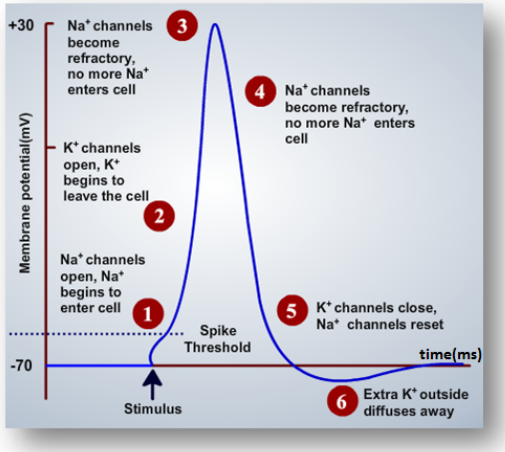

Figure 13: Membrane potential in time [21].

Until the resting potential is reached another signal cannot pass through the neuron.

The process, described above, was studied by Hodgkin and Huxley, using the so-called space clamping technique (see the Appendix), i.e., they kept the voltage constant along the axon. Otherwise, this process could be thought to happen at each point in the axon or at each Ranvier node (if the axon is myelinated). The action potential is first triggered at the soma end of the axon. When a part of an axon is depolarized, this depolarization spreads down the length of the axon. The propagation is described in Fig. 14.

2.2 Mathematical modelling of a nerve impulse through an unmyelinated axon

In the early 1950s, Alan Hodgkin and Andrew Huxley studied the membrane dynamics of the giant axon of the squid (Loligo) [13]. Although derived for a

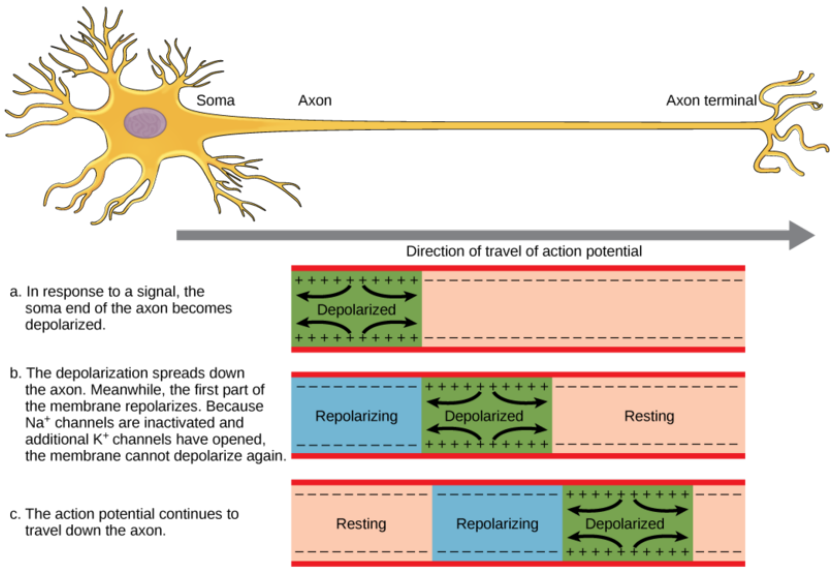

Figure 14: Action potential propagation in a nerve axon [22].

specific nerve, their mathematical model set the main concepts for the research in this field. Because the axon is a long thin projection, a 1D model is considered. Let us denote the spatial and time variables by $x \in [0, X]$ and $t \in [0, T]$, respectively.

2.2.1 Derivation of the Hodgkin–Huxley model

The mathematical model is based on the following two basic laws (for their derivation, see the Appendix) [13]:

- The charge conservation law:

$$j = -\frac{\partial i}{\partial x}, \tag{2}$$

where $i = i(x, t)$ is the longitudinal (x-directed) current at time t and point x of the axon (see Fig. 15), and

$$j(x, t) = j_c(x, t) + j_m(x, t) \tag{3}$$

is the total electric current per unit length of the fiber. It consists (as evident from the discussion in Section 2.1) of the transmembrane current, j_m (the ionic transport, primarily of K^+, Na^+ ions, through the voltage-gated channels), and the capacitive current, j_c (due to the properties of the axon membrane as a capacitor).

- Ohm's law:
$$i(x,t) = -\frac{1}{R}\frac{\partial V}{\partial x}(x,t), \tag{4}$$
where V is the transmembrane voltage and R is the longitudinal resistance per unit length of the fiber, which is assumed to be constant along the axon.

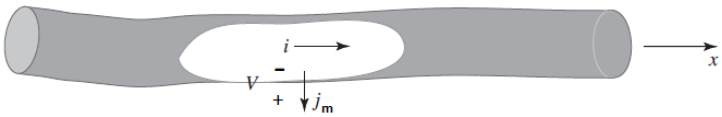

Figure 15: Electric current in an axon [13].

Combining equations (2), (3), and (4), the longitudinal current is eliminated to finally obtain the so-called **Cable equation**:

$$j_c + j_m = \frac{1}{R}\frac{\partial^2 V}{\partial x^2}. \tag{5}$$

To model the capacitive current, we differentiate eq. (1) and derive

$$j_c = \frac{\partial Q}{\partial t} = c\frac{\partial V}{\partial t}. \tag{6}$$

For the transmembrane current, Hodgkin and Huxley performed elaborate experiments for different voltages V (see the Appendix) and derived the following empirical expression [13]:

$$j_m = \underbrace{G_{Na}m^3h(V - V_{Na})}_{Na^+ \text{ current}} + \underbrace{G_K n^4(V - V_K)}_{K^+ \text{ current}} + \underbrace{G_L(V - V_L)}_{\text{leakage current}}, \tag{7}$$

where:

- G_{Na} and G_K are the maximum sodium and potassium conductances (or permeabilities) per unit area;
- V_{Na} and V_K are equilibrium voltages at which transmembrane sodium and potassium currents, respectively, are equal to 0;
- $m(x,t)$ is a "sodium turn-on" variable, which describes the opening of the Na^+ channels;
- $h(x,t)$ is a "sodium turn-off" variable, which describes the closing of the Na^+ channels;

- $n(x,t)$ is a potassium "turn-on" variable, which describes the opening of the K^+ channels.

The last term in (7) introduces a small leakage current, accounting for missed ionic measurements.

In their model, for the membrane turn-on and turn-off variables, Hodgkin and Huxley assumed that m, h, and n are the solutions of a system of first-order differential equations:

$$\begin{aligned}\frac{\partial m}{\partial t} &= -\frac{m - m_0(V)}{\tau_m(V)},\\ \frac{\partial h}{\partial t} &= -\frac{h - h_0(V)}{\tau_h(V)},\\ \frac{\partial n}{\partial t} &= -\frac{n - n_0(V)}{\tau_n(V)},\end{aligned} \tag{8}$$

where

$$\begin{aligned}m_0(V) &= \alpha_m/(\alpha_m + \beta_m),\\ \tau_m(V) &= 1/(\alpha_m + \beta_m),\\ h_0(V) &= \alpha_h/(\alpha_h + \beta_h),\\ \tau_h(V) &= 1/(\alpha_h + \beta_h),\\ n_0(V) &= \alpha_n/(\alpha_n + \beta_n),\\ \tau_n(V) &= 1/(\alpha_n + \beta_n).\end{aligned} \tag{9}$$

The coefficients in the above equations are measured at a given temperature of 6.8° (an additional scaling factor that accounts for changes in temperature could be introduced, but we do not include it here):

$$\begin{aligned}\alpha_m &= \frac{0.1(25 - V)}{\exp[(25 - V)/10] - 1},\\ \beta_m &= 4\exp[-V/18],\\ \alpha_h &= 0.07\exp[-V/20],\\ \beta_h &= \frac{1}{\exp[(30 - V)/10] + 1},\\ \alpha_n &= \frac{0.01(10 - V)}{\exp[(10 - V)/10] - 1},\\ \beta_n &= 0.125\exp[-V/80].\end{aligned} \tag{10}$$

Some additional intuition about m, n, and h is developed in the Appendix.

2.2.2 The Hodgkin–Huxley model

For convenience, we formulate here the complete model by coupling (5)–(8):

$$\begin{aligned}
\frac{1}{R}\frac{\partial^2 V}{\partial x^2} &= c\frac{\partial V}{\partial t} + j_m, && 0 < x < X,\ 0 < t \le T,\\
\frac{\partial m}{\partial t} &= -\frac{m - m_0(V)}{\tau_m(V)}, && 0 \le x \le X,\ 0 < t \le T,\\
\frac{\partial n}{\partial t} &= -\frac{n - n_0(V)}{\tau_n(V)}, && 0 \le x \le X,\ 0 < t \le T,\\
\frac{\partial h}{\partial t} &= -\frac{h - h_0(V)}{\tau_h(V)}, && 0 \le x \le X,\ 0 < t \le T,
\end{aligned} \tag{11}$$

where

$$j_m = G_{Na} m^3 h (V - V_{Na}) + G_K n^4 (V - V_K) + G_L (V - V_L).$$

The system is closed with initial conditions:

$$\begin{aligned}
V(x,0) &= V_{init}(x),\\
m(x,0) &= m_{init}(x),\\
n(x,0) &= n_{init}(x),\\
h(x,0) &= h_{init}(x),
\end{aligned} \tag{12}$$

for $x \in [0, X]$ and two boundary conditions for V. We shall later consider both Dirichlet and Neumann boundary conditions.

Remark. *Usually, it is assumed that the voltage is scaled, such that at resting state it is equal to 0. We shall follow the same convention.*

2.2.3 Numerical schemes

We shall derive a finite difference approximation of equations (11) and the corresponding initial and boundary conditions. Let us introduce a uniform mesh

$$\omega_{\Delta x,\Delta t} := \left\{ (x_i, t_j) : x_i = i\Delta x, t_j = j\Delta t, i = \overline{0,n}, j = \overline{0,m}, n = \frac{X}{\Delta x}, m = \frac{T}{\Delta t} \right\}.$$

We further denote the values of the approximate solutions for m, n, and h at node (x_i, t_j) with M_i^j, N_i^j, and H_i^j, respectively, and the approximate solution for the voltage V with Y_i^j.

Approximation of the main equations

We approximate the time derivatives in (11), using the forward difference formula, and the second spatial derivative with second order central difference formula [23]. Thus, we obtain the following explicit two-layer finite difference approximations:

$$\begin{aligned}
\frac{1}{R}\frac{Y_{i+1}^j - 2Y_i^j + Y_{i-1}^j}{\Delta x^2} &= c\frac{Y_i^{j+1} - Y_i^j}{\Delta t} + \tilde{j}_m(x_i, t_j),\ i = \overline{1, n-1},\ j = \overline{0, m-1},\\
\frac{M_i^{j+1} - M_i^j}{\Delta t} &= -\frac{M_i^j - m_0(Y_i^j)}{\tau_m(Y_i^j)}, \quad i = \overline{0, n}, \quad j = \overline{0, m-1},\\
\frac{H_i^{j+1} - H_i^j}{\Delta t} &= -\frac{H_i^j - h_0(Y_i^j)}{\tau_h(Y_i^j)}, \quad i = \overline{0, n}, \quad j = \overline{0, m-1},\\
\frac{N_i^{j+1} - N_i^j}{\Delta t} &= -\frac{N_i^j - n_0(Y_i^j)}{\tau_n(Y_i^j)}, \quad i = \overline{0, n}, \quad j = \overline{0, m-1},
\end{aligned}$$

where

$$\tilde{j}_m(x_i, t_j) := G_{Na}(M_i^j)^3 H_i^j \left(Y_i^j - V_{Na}\right) + G_K(N_i^j)^4(Y_i^j - V_K) + G_L(Y_i^j - V_L).$$

We rewrite the equations in the following form:

$$\begin{aligned}
Y_i^{j+1} &= \frac{\Delta t}{cR\Delta x^2}\left(Y_{i+1}^j + Y_{i-1}^j\right) + \left(1 - \frac{2\Delta t}{cR\Delta x^2}\right) Y_i^j - \frac{\Delta t}{c}\,\tilde{j}_m(x_i, t_j),\\
M_i^{j+1} &= \left(1 - \frac{\Delta t}{\tau_m(Y_i^j)}\right) M_i^j + \frac{\Delta t}{\tau_m(Y_i^j)} m_0(Y_i^j),\\
H_i^{j+1} &= \left(1 - \frac{\Delta t}{\tau_h(Y_i^j)}\right) H_i^j + \frac{\Delta t}{\tau_h(Y_i^j)} h_0(Y_i^j),\\
N_i^{j+1} &= \left(1 - \frac{\Delta t}{\tau_n(Y_i^j)}\right) N_i^j + \frac{\Delta t}{\tau_n(Y_i^j)} n_0(Y_i^j).
\end{aligned} \tag{13}$$

Approximation of the initial conditions

The initial conditions (12) are approximated exactly:

$$Y_i^0 = V_{init}(x_i), \quad M_i^0 = m_{init}(x_i), \quad N_i^0 = n_{init}(x_i), \quad H_i^0 = h_{init}(x_i), \tag{14}$$

for $i = \overline{0, n}$.

Approximation of the boundary conditions

- **Dirichlet boundary conditions**

  If we consider a Dirichlet boundary condition at $x = 0$, i.e.

  $$V(0,t) = V_{left}(t), \quad 0 \le t \le T,$$

  it can be approximated exactly as

  $$Y_0^j = V_{left}(t_j), \quad j = \overline{0,m}. \tag{15}$$

  Analogously, for Dirichlet boundary condition on the right boundary, we obtain

  $$Y_n^j = V_{right}(t_j), \quad j = \overline{0,m}.$$

- **Neumann boundary conditions**

  If we consider a Neumann boundary condition at $x = 0$, i.e.

  $$\frac{\partial V}{\partial x}(0,t) = V_{left}(t), \tag{16}$$

  we can approximate the spatial derivative by using first order forward difference formula and obtain

  $$\frac{Y_1^j - Y_0^j}{\Delta x} = V_{left}(t_j), \quad j = \overline{0,m}. \tag{17}$$

  The local approximation error (LAE) of the approximations (13) is $O(\Delta x^2 + \Delta t)$. However, if we use (17), the LAE of the whole finite difference scheme would degenerate to $O(\Delta x + \Delta t)$, because of the usage of the forward difference formula. Therefore, in order to increase the order of approximation of the boundary condition, we shall use a standard technique [23]. Let us denote V_i^j to mean the value of the exact solution V at the mesh point (x_i, t_j). Then, for the LAE of (17), using a Taylor expansion about $x = 0$, we consecutively obtain

  $$\begin{aligned}
  \psi_{\Delta x,\Delta t} &= \frac{V_1^j - V_0^j}{\Delta x} - V_{left}(t_j) \\
  &= \frac{1}{\Delta x}\left(V_0^j + \frac{\partial V}{\partial x}\Big|_0^j \Delta x + \frac{\partial^2 V}{\partial x^2}\Big|_0^j \frac{\Delta x^2}{2} + O(\Delta x^3) - V_0^j\right) - V_{left}(t_j) \\
  &= \frac{\Delta x}{2}\frac{\partial^2 V}{\partial x^2}\Big|_0^j + O(\Delta x^2).
  \end{aligned} \tag{18}$$

  Therefore, the following equality holds true:

  $$\frac{V_1^j - V_0^j}{\Delta x} - \frac{\Delta x}{2}\frac{\partial^2 V}{\partial x^2}\Big|_0^j = V_{left}(t_j) + O(\Delta x^2).$$

Finally, assuming that the cable equation (i.e., the first equation in (11)) is fulfilled also for $x = 0$ with a sufficient accuracy, we can express the second order spatial derivative in terms of the time derivative and obtain the following approximation with LAE $O(\Delta x^2 + \Delta t)$:

$$Y_0^{j+1} = \frac{2\Delta t}{cR\Delta x^2} Y_1^j + \left(1 - \frac{2\Delta t}{cR\Delta x^2}\right) Y_0^j - \frac{\Delta t}{c}\, \tilde{j}_m(x_0, t_j) - \frac{2\Delta t}{cR\Delta x} V_{left}(t_j),$$
$$j = \overline{0, m-1}. \tag{19}$$

Analogously, for a right Neumann boundary condition

$$\frac{\partial V}{\partial x}(X, t) = V_{right}(t),$$

we can obtain:

$$Y_n^{j+1} = \frac{2\Delta t}{cR\Delta x^2} Y_{n-1}^j + \left(1 - \frac{2\Delta t}{cR\Delta x^2}\right) Y_n^j - \frac{\Delta t}{c}\, \tilde{j}_m(x_n, t_j)$$
$$+ \frac{2\Delta t}{cR\Delta x} V_{right}(t_j), \quad j = \overline{0, m-1}. \tag{20}$$

2.2.4 Numerical experiments

In this section, we shall present numerical simulations based on the implementations of the finite difference schemes that we derived in the previous section, using CAS Wolfram Mathematica. On one hand, we shall, thus, validate the applicability of the proposed schemes and get a further intuition about the process of nerve impulse propagation. On the other hand, the simulated impulses could be used as an input for the modelling of calcium dynamics as discussed later in the thesis.

The model parameters, used for the numerical simulations, are shown in Table 1.

Parameter	Value	Parameter	Value
c	1 $\mu F/cm^2$	R	10Ω
G_{Na}	120 mmhos/cm^2	V_{Na}	115 mV
G_K	36 mmhos/cm^2	V_K	-12 mV
G_L	0.3 mmhos/cm^2	V_L	10 mV

Table 1: Parameters for the Hodgkin–Huxley model of an unmyelinated squid nerve cell's axon [13].

Experiment 1 (Single stimulus input)**.**
We consider the following initial and boundary conditions for the model (11):

$$\begin{aligned} &V(x,0) = \frac{100}{\sqrt{\pi}} e^{-(x/5)^2}, \frac{\partial V}{\partial x}(0,t) = \frac{\partial V}{\partial x}(X,t) = 0, \\ &m(x,0) = m_0(0),\ n(x,0) = n_0(0),\ h(x,0) = h_0(0). \end{aligned} \tag{21}$$

As an initial condition for V, we have used Gaussian bell curve, while as initial conditions for m, n, and h we have chosen their resting states. We model the situation, when the initial segment of the axon has been depolarized and we simulate a single action potential. Thus, we implement the finite difference scheme (13), (14), (19), and (20), where the numerical domain $x \in [0, 10]$, $t \in [0, 30]$ is discretized with $\Delta x = 0.1$ and $\Delta t = 0.005$.

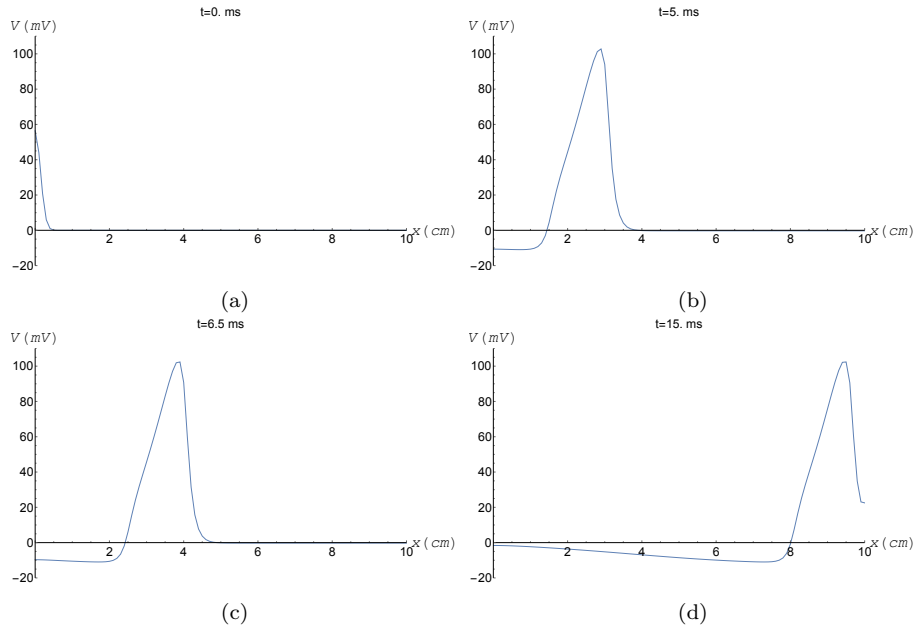

Figure 16: Experiment 1: Nerve impulse propagation.

Numerical results are obtained by using CAS Wolfram Mathematica and are shown in Fig. 16. The results show that the nerve impulse is transmitted as a travelling wave. In response to the initial stimulus, the beginning of the axon is depolarized. Further, this depolarization is spread along the axon, while the segments adjacent on the left to the wave front are getting repolarized and then hyperpolarized. In Fig. 16(d), on the left boundary, the axon is returning to its resting state.

Experiment 2 (Square wave stimulus input)**.**
We consider the following initial and boundary conditions for the model (11):

$$\begin{aligned} &V(x,0)=0, \quad V(0,t)=\mu(t), \quad \frac{\partial V}{\partial x}(X,t)=0, \\ &m(x,0)=m_0(0),\ n(x,0)=n_0(0),\ h(x,0)=h_0(0), \end{aligned} \tag{22}$$

where $\mu(t)$ is a piecewise constant function, which is chosen to describe a periodic impulse signal. The latter function is depicted in Fig. 17. The simulation of

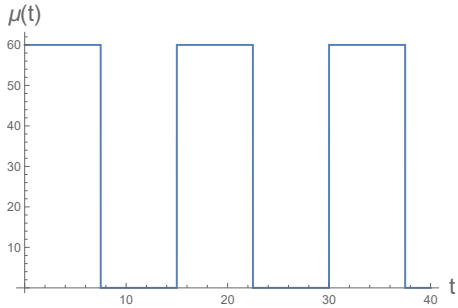

Figure 17: Experiment 2: The graph of the function $\mu(t)$, which is imposed as a boundary condition.

nerve impulse propagation, based on the finite difference scheme (13), (14), (15), and (20), for $X = 20$ is shown in Fig. 18. As can be seen in the latter, the boundary condition on the left boundary, imposed with the function $\mu(t)$, generates impulses on a periodic range of time. Let us note that in order for another impulse to be generated, the left boundary of the axon should be first returned to a resting state.

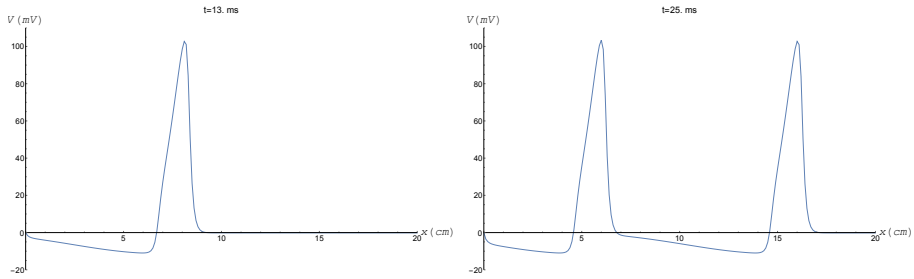

(a) (b)

Figure 18: Experiment 2: Nerve impulse propagation.

Experiment 3 (Weak initial stimulus)**.**
We consider the following initial and boundary conditions for the model (11):

$$\begin{aligned} V(x,0) &= \frac{25}{\sqrt{\pi}} e^{-(x/5)^2}, \quad \frac{\partial V}{\partial x}(0,t) = \frac{\partial V}{\partial x}(X,t) = 0, \\ m(x,0) &= m_0(0),\ n(x,0) = n_0(0),\ h(x,0) = h_0(0). \end{aligned} \tag{23}$$

Numerical results for $X = 5$ are presented in Fig. 19. Since the initial stimulus is not strong enough, a nerve impulse is not transmitted through the axon. Thus, the axon quickly returns to its resting state.

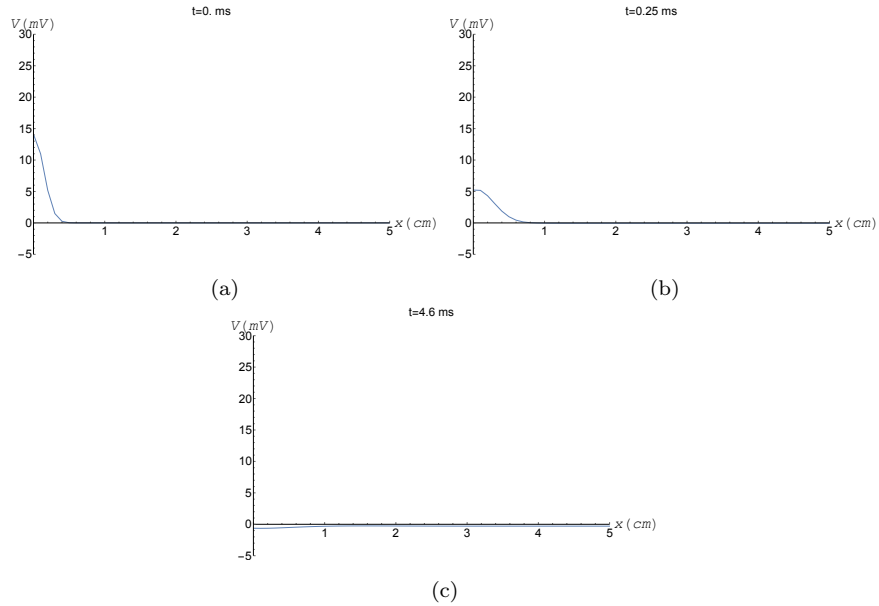

Figure 19: Experiment 3: Nerve impulse propagation.

2.3 Mathematical modelling of a nerve impulse through a myelinated axon

In the peripheral nervous system, motor neurons are covered with the so-called myelin sheath. The myelin sheath of the neuron's axon is a substance, rich in lipids, which helps for the proper functioning of the motor neuron by providing insulation and protection from the environment, reducing the membrane capacitance and speeding the nerve impulse propagation through the axon. The sheath of myelin is not continuous along the axon of the neuron—it is interrupted periodically at myelin-sheath gaps, called Ranvier nodes. Since the

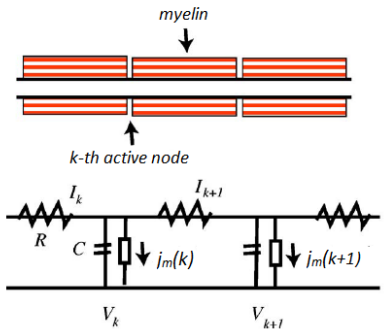

Figure 20: Structure of a myelinated nerve fiber and its corresponding electrical circuit [26].

myelinated axon can be very long, it could contain hundreds or thousands of Ranvier nodes. When an impulse is propagated along a myelinated axon, it "jumps" from node to node, which is known as saltatory propagation of impulses [24]. **Often the nerve propagation failure is due to some damage of the covering myelin sheath**. A typical motor neuron structure was shown in Fig. 4.

2.3.1 The discrete Hodgkin–Huxley model

The myelin sheath allows the axon to conduct neuroelectric signals by exciting only a small percentage of the membrane—the one that is exposed to the extracellular medium at the nodes of Ranvier, see [25]. Most of the mathematical models for myelinated axons assume that the membrane resistance is so high and has such a low capacitance that it fully isolates the membrane of the axon. The latter is referred to as pure saltatory theory. Thus, when a membrane is depolarized at a certain Ranvier node, we shall assume that it does not tend to depolarize the adjacent part of the axon, but it excites the membrane at the next node.

To model the nerve propagation in this case, we shall consider a spatially discrete Hodgkin–Huxley system that was described by R. Fitzhugh in [24] and A. Carpio in [26].

Derivation of the main equations

The behavior of the nerve impulse transmission can be described by a lumped element model of electrical circuits, see Fig. 20. Let $k = \overline{0, n}$ denote the index of the corresponding Ranvier node (see Fig. 20). To model the nerve transmission,

we shall apply Kirchhoff's current law, which states that the current, flowing into a node, is equal to the current, flowing out. Therefore, if we consider the k-th Ranvier node in an axon, we can write

$$I_k = I_{k+1} + j(k), \tag{24}$$

where I_k and I_{k+1} are the currents flowing in and out of the k-th Ranvier node and

$$j(k) = j_c(k) + j_m(k)$$

is the sum of the transmembrane and the capacitive current at the k-th node. Analogously, one can apply Kirchhoff's voltage law[2], combined with Ohm's law, to obtain

$$V_{k-1} - V_k = RI_k, \tag{25}$$

where V_k is the membrane voltage at the k-th node and R is the resistance of the axonal membrane. By expressing I_k and I_{k+1} at the internal nodes, using (25), and substituting in (24), we derive

$$\begin{aligned} c\frac{dV_k}{dt} &= \frac{1}{R}\left(V_{k+1} - 2V_k + V_{k-1}\right) - j_m(V_k, m_k, h_k, n_k), \quad k = \overline{1, n-1}, \\ j_m &= G_{Na} m_k^3 h_k (V_k - V_{Na}) + G_K n_k^4 (V_k - V_K) + G_L (V_k - V_L). \end{aligned} \tag{26}$$

In the case of $k = 0$, for our numerical experiments, we shall consider two different conditions:

- $V_0(t) = V_{left}(t)$—an analogue of the Dirichlet condition;
- A discrete analogue of a no-flux boundary condition:

$$c\frac{dV_0}{dt} + j_m(V_0, m_0, n_0, h_0) = \frac{V_1 - V_0}{R}. \tag{27}$$

  The latter is derived by using Kirchoff's laws at $k = 0$ and assuming that $I_0 = 0$:

$$\begin{aligned} c\frac{dV_0}{dt} + j_m(V_0, m_0, n_0, h_0) &= -I_1 \\ -V_1 + V_0 &= RI_1. \end{aligned}$$

Analogous conditions can be imposed for $k = n$.

Similarly to Section 2.2, m_k, n_k, and h_k, $k = \overline{0, n}$, satisfy the system

$$\begin{aligned} \frac{dm_k}{dt} &= -\frac{m_k - \tilde{m}_0(V_k)}{\tilde{\tau}_m(V_k)}, \\ \frac{dn_k}{dt} &= -\frac{n_k - \tilde{n}_0(V_k)}{\tilde{\tau}_n(V_k)}, \\ \frac{dh_k}{dt} &= -\frac{h_k - \tilde{h}_0(V_k)}{\tilde{\tau}_h(V_k)}, \end{aligned} \tag{28}$$

[2]The directed sum of the potential differences (voltages) around any closed loop is zero [27].

where $\tilde{m}_0,\ \tilde{h}_0,\ \tilde{n}_0,\ \tilde{\tau}_m,\ \tilde{\tau}_n,\ \tilde{\tau}_h$ are $m_0,\ h_0,\ n_0,\ \tau_m,\ \tau_n,\ \tau_h$ from (9).

2.3.2 Numerical experiments

We solve the ODE system (26), (28) for $t \in [0, 50]$, closed with corresponding conditions, using the forward Euler method with a time-discretization step $\Delta t = 0.005$. For our numerical experiments we shall compare the propagation of nerve impulses in myelinated and unmyelinated axons, using again the parameters, considered in Table 1.

Experiment 1 (Single stimulus input)**.**
We consider the following conditions for the ODE system (26), (28):

$$\begin{aligned} &V_k(0) = \frac{4}{\sqrt{\pi}} e^{-(2k/5)^2},\ m_k(0) = \tilde{m}_0(0), \\ &n_k(0) = \tilde{n}_0(0),\ h_k(0) = \tilde{h}_0(0),\ k = \overline{0,n}, \\ &c\frac{dV_0}{dt} + j_m(V_0, m_0, n_0, h_0) = \frac{V_1 - V_0}{R}, \\ &c\frac{dV_n}{dt} + j_m(V_n, m_n, n_n, h_n) = \frac{V_{n-1} - V_n}{R}. \end{aligned} \tag{29}$$

Similarly to Section 2.2.4, as an initial condition for the voltage V at the k-th Ranvier node, i.e., V_k, we have considered a "discrete Gaussian bell curve", defined only at the Ranvier nodes, while as initial conditions for m_k, n_k and h_k we have used their resting states. We model the case when the initial segment is depolarized, in result of a single stimulus. The numerical results are shown in Fig. 21. For visualization purposes, we have interpolated between the values at the Ranvier nodes in the case of a myelinated axon. Let us note that the k-th Ranvier node is assumed to be at $x = 2k,\ k = \overline{0,n}$. As can be seen in the latter figure, the myelin sheath on the nerve cell's axon significantly improves the speed of the nerve impulse propagation.

Experiment 2 (Square wave stimulus)**.**
The difference with the previous experiment is only that we shall consider a periodic stimulus on the left boundary of the axon, modelled by the piecewise constant function $\mu(t)$, described in the previous section and depicted in Fig. 17.

The numerical results are shown in Fig. 22. Analogously to the single impulse simulation, the results show that the myelin sheath of the axon improves the speed of nerve impulse propagation. As evident from Fig. 22(d), in the unmyelinated axon the first impulse is still propagating, when the second one is generated, while on the myelinated axon the first impulse has been transmitted and the second one is quickly reaching the end of the axon.

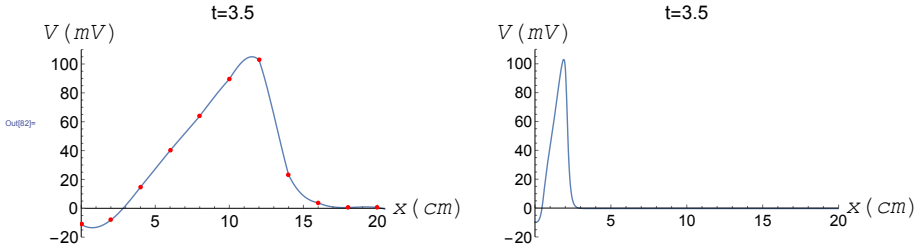

(a)

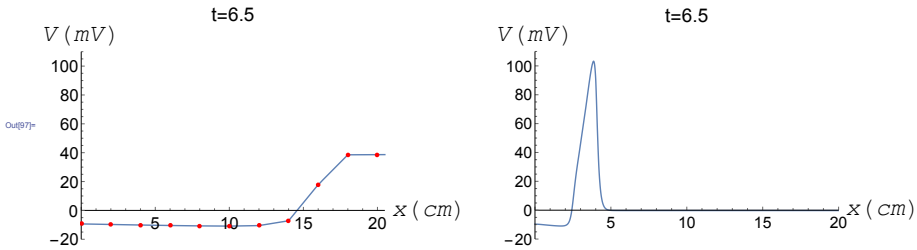

(b)

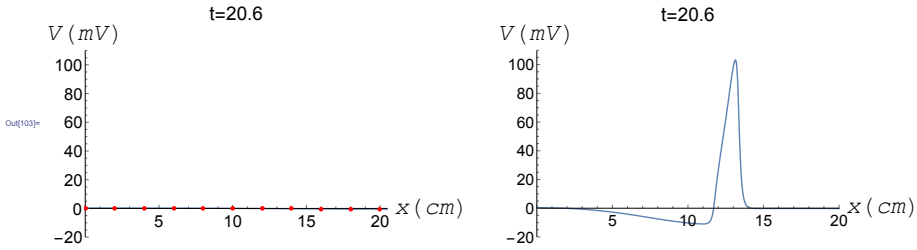

(c)

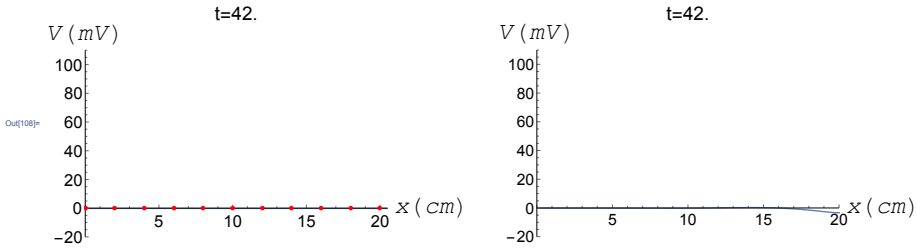

(d)

Figure 21: Experiment 1: Comparison between the myelinated (left) and unmyelinated (right) neuron for a single stimulus.

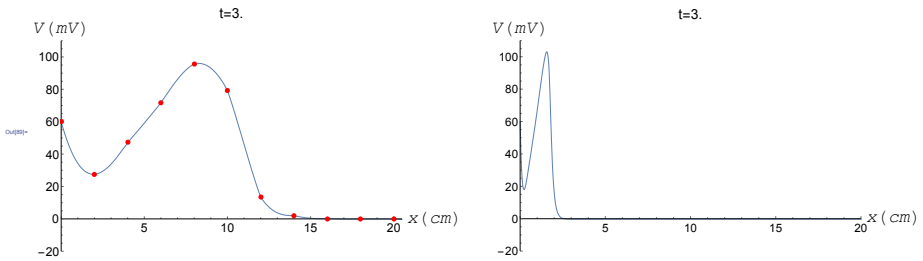

(a)

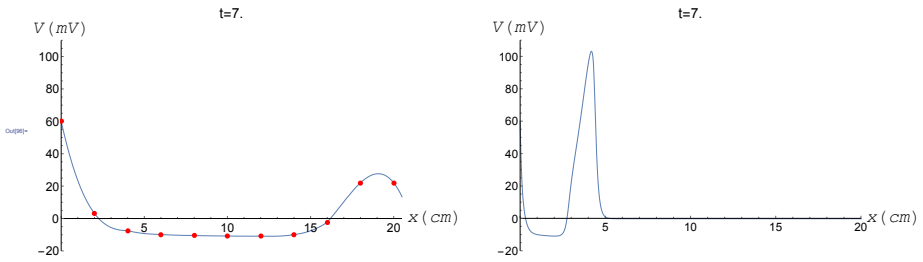

(b)

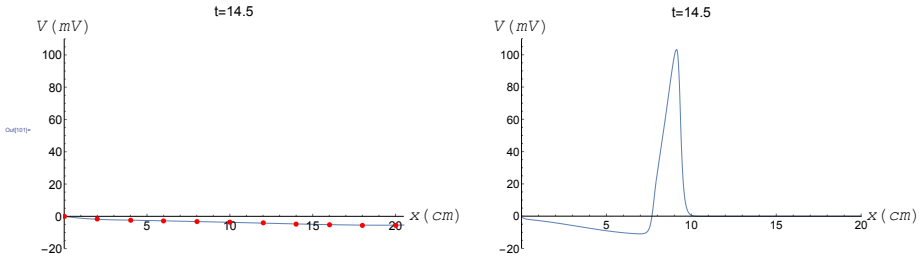

(c)

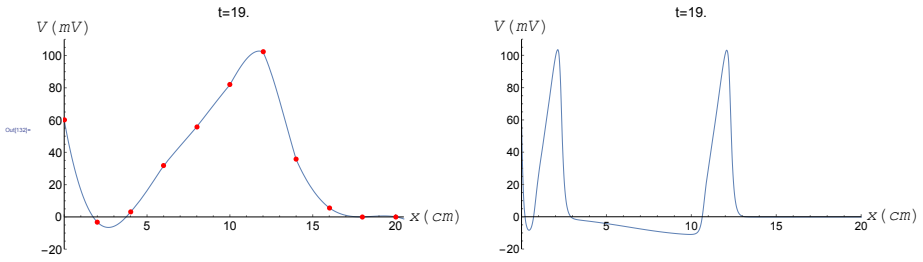

(d)

Figure 22: Experiment 2: Comparison between the myelinated (left) and unmyelinated (right) axon for a periodic stimulus.

2.4 Conclusion and discussion

In this section, we have derived the classical Hodgkin–Huxley model for the neural impulse propagation along a nerve's axon and its modification, described in terms of differential-difference equations, for the case of myelinated axons. We have carried out numerical experiments in both cases for biologically relevant values of the model parameters. As evident from them, the myelin sheath of the axon highly improves the speed of propagation of the nerve impulses. Therefore, destroying the myelin sheath (which is one possible malfunctioning, connected with neuromuscular diseases) could be very harmful for the normal functioning of the neuromuscular system. The considered models allow to study those effects, by simulating the case of (partially) demyelinated axons, which is a direction for our future studies. Furthermore, since it is well known that using the Hodgkin–Huxley model is very expensive from a computational point of view, one could consider some of its simplifications. In particular, we shall mention the Fitzhugh–Nagumo model that is often used for obtaining qualitative information about the neural impulse propagation (see, e.g., [13] and the references therein).

3 Modelling of calcium dynamics

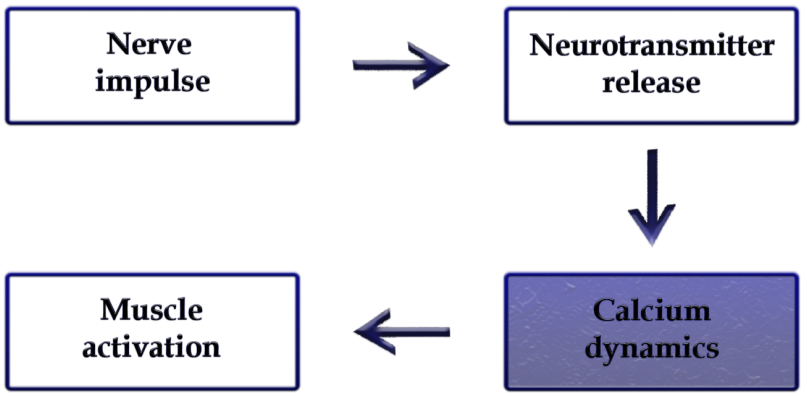

In this section, we shall study a model for the calcium dynamics in the muscle cell, based on mass action kinetics. The latter is a result from the nerve impulse transmission in a nerve cell and the transported neurotransmitter in the neuromuscular junction, which will be discussed in Section 4. A brief description of the process was given in Sections 1.1.1 and 1.2.

The main results in this section are also published in [28].

3.1 Mathematical model

As discussed earlier, when a nerve impulse comes to the muscle, the action potential results in the release of Ca^{2+} ions from the SR. Ca^{2+} ions then flow into the sarcomere where the CFs are situated. Then, Ca^{2+} ions start binding to the receptors in the CFs and as a result, the filaments start sliding, causing the sarcomere to shorten. When the stimulus is turned off, the Ca^{2+} ions are transported back into the SR and the sarcomere relaxes. Having in mind the aforementioned, one needs to model the dynamics of calcium ions, sarcoplasmic reticulum (SR), and contractile filaments (CFs), in order to understand the process of muscle contraction.

For this purpose, we consider a mass action kinetics model, proposed by Williams [29], further considered by McMillen [30] and used by Meredith in [9]. The model is based on the principle of mass action kinetics, which assumes that the rate of a chemical reaction is proportional to the concentration of the reactants. Let us denote the following, see Fig. 23:

- c—concentration of free calcium ions;
- r_u—concentration of unbound sarcoplasmic reticulum sites;
- r_b—concentration of bound sarcoplasmic reticulum sites;
- f_u—concentration of unbound CF sites;
- f_b—concentration of bound CF sites;
- k_1—rate of release of calcium ions from the SR;
- k_2—rate of binding of calcium ions to the SR;
- k_3—rate of binding of calcium ions to the CFs;
- k_4—rate of release of calcium ions from the CFs.

The kinetic scheme of calcium dynamics is illustrated in Fig. 23: Based on the

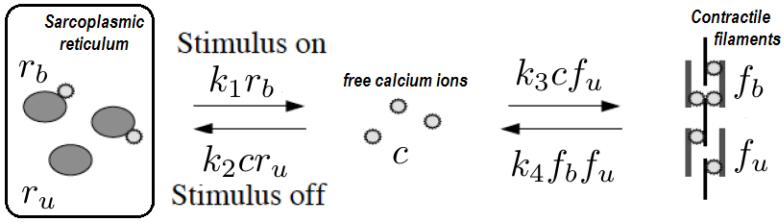

Figure 23: Kinetic scheme for calcium dynamics [29].

principle of mass action, the following statements are valid:

1. When the stimulus is on, i.e., when there is an action potential in the muscle cell, the rate of unbinding of calcium ions from the SR is proportional to the concentration of calcium-bound SR sites with a rate constant k_1;

2. When the stimulus is off, the rate of binding of calcium ions to the SR is proportional to the product of the concentrations of free calcium ions and unbound SR calcium-binding sites with a rate constant k_2;

3. The rate of binding of calcium ions to the CF is proportional to the product of the concentrations of free calcium ions and unbound filament sites with a rate constant k_3.

Further, because of empirical evidence, the rate of release of calcium ions from the CF is chosen to be proportional to the product of concentration of bound and unbound filament sites with a rate constant k_4. This is meant to account for some cooperativity between the bound and unbound CF sites in the process of calcium release.

In mathematical terms, the above assumptions result in the following system of five ODEs:

$$\begin{aligned}
\frac{dc}{dt} &= k_1 r_b - k_2 r_u c - k_3 f_u c + k_4 f_b f_u, \\
\frac{dr_b}{dt} &= -k_1 r_b + k_2 r_u c, \\
\frac{dr_u}{dt} &= k_1 r_b - k_2 r_u c, \\
\frac{df_b}{dt} &= k_3 c f_u - k_4 f_b f_u, \\
\frac{df_u}{dt} &= -k_3 c f_u + k_4 f_b f_u,
\end{aligned} \tag{30}$$

where k_1 and k_2 are non-negative coefficients and k_3, k_4 are positive constants. Further, the following assumptions are made by Williams [29]:

1. when the stimulus is on, $k_1 > 0,\ k_2 = 0$;

2. when the stimulus is off, $k_1 = 0, k_2 > 0$;

3. the total amount of calcium is constant:

$$c + f_b + r_b = C; \tag{31}$$

4. the total numbers of bound and unbound SR and CF sites are constant, i.e,

$$\begin{aligned}
r_u + r_b &= S, \\
f_b + f_u &= F,
\end{aligned} \tag{32}$$

where S and F are the total numbers of SR and CF sites.

By using assumptions (31)–(32), we reduce the ODE system (30) to the following two-dimensional model for the concentrations of free calcium ions and calcium-bound sites:

$$\begin{aligned}\frac{dc}{dt} &= (k_4 f_b - k_3 c)(F - f_b) + k_1 (C - c - f_b) + k_2 c (C - S - c - f_b),\\ \frac{df_b}{dt} &= -(k_4 f_b - k_3 c)(F - f_b).\end{aligned} \tag{33}$$

Further, we scale the model by the total amount of the CF sites F:

$$\begin{aligned}&\hat{f}_b = f_b/F, \quad \hat{c} = c/F, \quad \hat{C} = C/F, \quad \hat{S} = S/F,\\ &\hat{k}_2 = Fk_2, \quad \hat{k}_3 = Fk_3, \quad \hat{k}_4 = Fk_4.\end{aligned} \tag{34}$$

Substituting (34) in (33) and skipping the hats for notational simplicity, we obtain

$$\begin{aligned}\frac{dc}{dt} &= (k_4 f_b - k_3 c)(1 - f_b) + k_1 (C - c - f_b) + k_2 c (C - S - c - f_b),\\ \frac{df_b}{dt} &= -(k_4 f_b - k_3 c)(1 - f_b).\end{aligned} \tag{35}$$

Remark. *The above scaling leads to certain restrictions for f_b and c, which we shall use later in the qualitative analysis of the system* (35)*. Dividing both sides of* (31) *and* (32) *by F, we derive:*

$$\begin{aligned}\hat{c} + \hat{f}_b + \hat{r}_b &= \hat{C},\\ \hat{f}_b + \hat{f}_u &= 1.\end{aligned}$$

From the latter equations and $\hat{c} \geq 0,\ \hat{f}_b \geq 0,\ \hat{r}_b \geq 0,\ \hat{f}_u \geq 0$, we obtain the restrictions

$$\begin{aligned}0 \leq \hat{c} + \hat{f}_b &\leq \hat{C},\\ 0 \leq \hat{f}_b &\leq 1.\end{aligned}$$

Therefore, system (35) *is considered in the phase space*

$$\{(c, f_b) \in \mathbb{R}^2 :\ 0 \leq c + f_b \leq C,\ 0 \leq f_b \leq 1,\ c \geq 0\}. \tag{36}$$

3.2 Qualitative analysis of model's dynamics in the limiting cases $k_1 = 0$, $k_2 = 0$

In this section, we shall study qualitatively the system of differential equations (35). Some basic notions from the theory of dynamical systems is given in the Appendix. We shall consider the two limiting cases—when the stimulus is on, i.e., when $k_2 = 0,\ k_1 > 0$, and when the stimulus is off, i.e., $k_1 = 0,\ k_2 > 0$.

3.2.1 Case $k_1 > 0,\ k_2 = 0$.

Let us first consider the case when the rate constant for binding of calcium to the sarcoplasmic reticulum (SR) k_2 is equal to zero. Thus, the system we consider is:

$$\begin{aligned} \frac{dc}{dt} &= (k_4 f_b - k_3 c)(1 - f_b) + k_1 (C - c - f_b), \\ \frac{df_b}{dt} &= -(k_4 f_b - k_3 c)(1 - f_b). \end{aligned} \tag{37}$$

Existence of equilibrium points

The equilibria of the system (37) are the solutions of the system of algebraic equations

$$\begin{aligned} (k_4 f_b - k_3 c)(1 - f_b) + k_1 (C - c - f_b) &= 0, \\ -(k_4 f_b - k_3 c)(1 - f_b) &= 0. \end{aligned}$$

Solving the latter system, we find two possible equilibrium points:

$$E_1 = (C - 1, 1) \text{ and } E_2 = \left(\frac{Ck_4}{k_3 + k_4}, \frac{Ck_3}{k_3 + k_4} \right).$$

First, let us consider the conditions for the existence of the equilibrium points.

Proposition 1. *The equilibrium point E_1 exists iff $C \geq 1$. The equilibrium point E_2 exists exactly when $0 \leq C \leq \dfrac{k_3 + k_4}{k_3}$.*

Proof. In order for the equilibrium points to exist (i.e., to be in the phase space) they must satisfy the restrictions (36). Therefore, we substitute the concentrations for c and f_b, corresponding to the two equilibrium points, to obtain conditions for their existence.

- Equilibrium $E_1 = (C - 1, 1)$.
  We substitute $c = C - 1$ and $f_b = 1$ in (36) and derive the existence condition $C \geq 1$.
- Equilibrium $E_2 = \left(\dfrac{Ck_4}{k_3 + k_4}, \dfrac{Ck_3}{k_3 + k_4} \right)$.
  We substitute the latter in (36) and derive:

$$\begin{aligned} 0 \leq & \frac{Ck_4}{k_3 + k_4} + \frac{Ck_3}{k_3 + k_4} \leq C, \\ 0 \leq & \frac{Ck_3}{k_3 + k_4} \leq 1. \end{aligned}$$

The first inequalities are trivially fulfilled, while the latter one is satisfied for $0 \leq C \leq \dfrac{k_3 + k_4}{k_3}$. □

Local stability of equilibrium points

To analyze the local stability of the equilibrium points we use the Hartman–Grobman theorem, i.e., we consider the linearization of the system about each of them and analyze the corresponding linear systems (see the Appendix). The Jacobi matrix of (37) as a function of the phase variables c and f_b is:

$$J(c, f_b) = \begin{pmatrix} -k_3(1-f_b) - k_1 & k_4(1-f_b) - k_4 f_b + k_3 c - k_1 \\ k_3(1-f_b) & -k_4(1-f_b) + k_4 f_b - k_3 c \end{pmatrix}.$$

Proposition 2. *The conditions for the stability of the equilibrium points E_1 and E_2 are given in Table 2, where C is chosen as a bifurcation parameter.*

C	$0 < C < 1$	$1 < C < \dfrac{k_3 + k_4}{k_3}$	$C > \dfrac{k_3 + k_4}{k_3}$
E_1	∄	saddle	stable
E_2	stable	stable	∄

Table 2: Classification of equilibria for the case $k_2 = 0$ in terms of C.

Proof. We shall analyze the stability of the equilibrium points separately.

1. Local stability of $E_1 = (C-1, 1)$.
   As derived in Proposition 1, the condition for the existence of the equilibrium point is $C \geq 1$. Substituting E_1 in the Jacobi matrix, we derive:

   $$J(E_1) = \begin{pmatrix} -k_1 & -k_4 + k_3(C-1) - k_1 \\ 0 & k_4 - k_3\,(C-1) \end{pmatrix}.$$

   For the eigenvalues $\lambda_1,\ \lambda_2$ of $J(E_1)$, we have

   $$\lambda_1 = -k_1 < 0,\ \lambda_2 = k_4 - k_3(C-1).$$

   Using the latter, we consider two cases for determining the stability of E_1:

   - $k_4 - k_3\,(C-1) > 0 \iff C < \dfrac{k_3 + k_4}{k_3}$.
     In this case, the eigenvalues are with opposite signs. That is, the equilibrium is a saddle point.

- $k_4 - k_3\,(C-1) < 0 \iff C > \dfrac{k_3+k_4}{k_3}$
  In this case, both eigenvalues are negative and E_1 is asymptotically stable.

2. Local stability of $E_2 = \left(\dfrac{Ck_4}{k_3+k_4}, \dfrac{Ck_3}{k_3+k_4}\right)$.
   We compute the Jacobi matrix at E_2:

$$J(E_2) = \begin{pmatrix} -k_3\left(1-\dfrac{Ck_3}{k_3+k_4}\right) - k_1 & k_4\left(1-\dfrac{Ck_3}{k_3+k_4}\right) - k_1 \\ k_3\left(1-\dfrac{Ck_3}{k_3+k_4}\right) & -k_4\left(1-\dfrac{Ck_3}{k_3+k_4}\right) \end{pmatrix}$$

   and obtain

$$\lambda_1\lambda_2 = detJ(E_2) = k_1\,(k_4 - k_3(C-1))\,,$$
$$\lambda_1 + \lambda_2 = traceJ(E_2) = -k_1 - k_4 + k_3\,(C-1)\,.$$

   By the existence condition for E_2, derived in Proposition 1, we conclude that the determinant is always positive, with $\lambda_1 + \lambda_2 < 0$ and, therefore, the equilibrium is asymptotically stable, whenever it exists. □

Numerical experiments

In this section, we give example phase portraits for the three different cases, considered in the classification of the equilibria in Proposition 2. For the numerical experiments, we consider the model parameters, taken from Table 5:

$$k_1 = 9.6,\ k_3 = 65,\ k_4 = 45,$$

and $S = 2$. Let us note that the initial conditions for the system (37) must satisfy conditions (36).

Experiment 1. We consider the following parameter value—$C = 0.8$, which corresponds to the case $0 < C < 1$. Thus, as concluded in Proposition 2, in this case the point $E_1 = (C-1, 1)$ does not exist, while $E_2 = \left(\dfrac{k_4C}{k_3+k_4}, \dfrac{k_3C}{k_3+k_4}\right)$ is asymptotically stable. The numerical results are shown in Fig. 24 and confirm the analytical conclusions.

Experiment 2. We consider the parameter $C = 1.6$, which corresponds to the case $1 < C < \dfrac{k_3+k_4}{k_3}$. By Proposition 2, in this case the equilibrium point

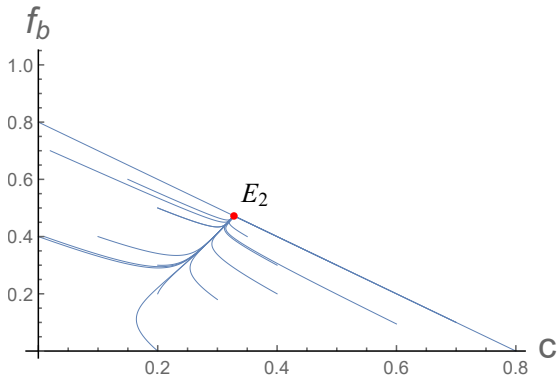

Figure 24: Phase portrait for the case $k_2 = 0$ with parameter value $C = 0.8$. E_1 does not exist, while E_2 is a stable equilibrium.

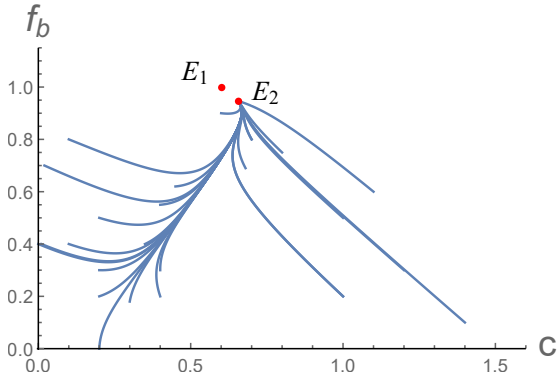

Figure 25: Phase portrait for the case $k_2 = 0$ with parameter value $C = 1.6$. E_1 is a saddle point, E_2 is a stable equilibrium.

$E_1 = (C-1, 1)$ is a saddle point, while $E_2 = \left(\frac{k_4 C}{k_3+k_4}, \frac{k_3 C}{k_3+k_4}\right)$ is again asymptotically stable. The numerical results confirm the conclusions in the Proposition and are depicted in Fig. 25.

Experiment 3. In this experiment, we consider the parameter $C = 2$, which corresponds to the case $C > \frac{k_3+k_4}{k_3}$. Following Proposition 2, $E_1 = (C-1, 1)$ is to be asymptotically stable, while $E_2 = \left(\frac{k_4 C}{k_3+k_4}, \frac{k_3 C}{k_3+k_4}\right)$ does not exist. The numerical results are shown in Fig. 26. Again, the numerical experiments are in agreement with the analytic results.

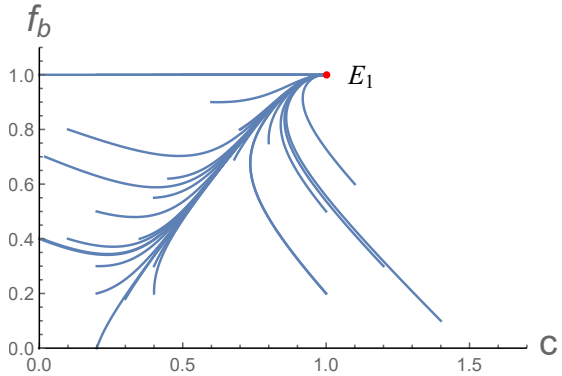

Figure 26: Phase portrait for the case $k_2 = 0$ with parameter value $C = 2$. E_1 is a stable equilibrium, E_2 does not exists.

Remark. *By the corresponding results in Fig 24, 25, and 26, we can further suppose that the locally stable equilibrium points in each of the considered experiments are also globally asymptotically stable.*

3.2.2 Case $k_1 = 0,\ k_2 > 0$.

Let us now consider the case, when the rate constant for release of calcium from the sarcoplasmic reticulum (SR), k_1, is equal to zero. Thus, we consider the following system:

$$\begin{aligned} \frac{dc}{dt} &= (k_4 f_b - k_3 c)(1 - f_b) + k_2 c\,(C - S - c - f_b)\,, \\ \frac{df_b}{dt} &= -(k_4 f_b - k_3 c)(1 - f_b)\,. \end{aligned} \tag{38}$$

Existence of equilibrium points

To find the equilibrium points of the latter system of ODEs, we solve the system of algebraic equations

$$(k_4 f_b - k_3 c)(1 - f_b) + k_2 c\,(C - S - c - f_b) = 0, \tag{39}$$

$$-(k_4 f_b - k_3 c)(1 - f_b) = 0. \tag{40}$$

The solutions of (40) are $f_b = 1$ and $f_b = \dfrac{k_3}{k_4}\,c$. Substituting the latter in (39), we derive the following four solutions of the system (39)–(40) and, therefore,

four possible equilibrium points to the system (38):

$$E_1 = (0,1),\ E_2 = (C-S-1,1),\ E_3 = (0,0),\ E_4 = \left(\frac{k_4(C-S)}{k_3+k_4}, \frac{k_3(C-S)}{k_3+k_4}\right).$$

We shall derive conditions for the existence of each of the equilibrium points E_1–E_4 in terms of the total amount of calcium C.

Proposition 3. *The following statements are valid:*

- *Equilibrium point E_1 exists exactly when $C \geq 1$;*
- *Equilibrium points E_2 exists if and only if $C \geq S+1$;*
- *Equilibrium point E_3 exists for every choice of the parameters in the model (38);*
- *Equilibrium point E_4 exists iff $S \leq C \leq S + \dfrac{k_3+k_4}{k_3}$.*

Proof. We shall derive the conditions for the existence of the equilibrium points separately.

1. Existence of $E_1 = (0,1)$.
   Taking into consideration the inequalities in (36) and substituting $c = 0$ and $f_b = 1$, we obtain the condition $C \geq 1$.

2. Existence of $E_2 = (C-S-1,1)$.
   We substitute the values for c and f_b in (36) and derive $C - S - 1 \geq 0 \iff C \geq S+1$.

3. Existence of $E_3 = (0,0)$.
   The existence of this equilibrium is trivial since the point (0,0) satisfies the conditions in (36) and, therefore, exists for every choice of the parameters in the model (38).

4. Existence of $E_4 = \left(\dfrac{k_4(C-S)}{k_3+k_4}, \dfrac{k_3(C-S)}{k_3+k_4}\right)$.
   Substituting the latter in the inequalities in (36), we derive

$$0 \leq \frac{k_4(C-S)}{k_3+k_4} + \frac{k_3(C-S)}{k_3+k_4} \leq C$$
$$0 \leq \frac{k_3(C-S)}{k_3+k_4} \leq 1.$$

   Taking into consideration the positivity of the constants k_3, k_4, we derive the condition $S \leq C \leq S + \dfrac{k_3+k_4}{k_3}$. □

Local stability of equilibrium points

Proposition 4. *The conditions for the stability of the equilibrium points* $E_1 = (0,1),\ E_2 = (C-S-1,1),\ E_3 = (0,0),$ *and* $E_4 = \left(\frac{k_4(C-S)}{k_3+k_4}, \frac{k_3(C-S)}{k_3+k_4}\right)$ *of the system* (38)*, where* C *is chosen as a bifurcation parameter, given in Table 3 for the case* $S<1$ *and in Table 4 for the case* $S>1$*, are valid.*

C	$0<C<S$	$S<C<1$	$1<C<S+1$	$S+1<C<S+\frac{k_3+k_4}{k_3}$	$C>S+\frac{k_3+k_4}{k_3}$
E_1	$\nexists$	$\nexists$	saddle	unstable	unstable
E_2	$\nexists$	$\nexists$	$\nexists$	saddle	stable
E_3	stable	saddle	saddle	saddle	saddle
E_4	$\nexists$	stable	stable	stable	$\nexists$

Table 3: Classification of equilibria for the case $k_1 = 0$ in terms of the total amount of calcium ions C, when $S<1$ holds.

C	$0<C<1$	$1<C<S$	$S<C<S+1$	$S+1<C<S+\frac{k_3+k_4}{k_3}$	$C>S+\frac{k_3+k_4}{k_3}$
E_1	$\nexists$	saddle	saddle	unstable	unstable
E_2	$\nexists$	$\nexists$	$\nexists$	saddle	stable
E_3	stable	stable	saddle	saddle	saddle
E_4	$\nexists$	$\nexists$	stable	stable	$\nexists$

Table 4: Classification of equilibria for the case $k_1 = 0$ in terms of the total amount of calcium ions C, when $S>1$ is valid.

Proof. Let us consider the four possible equilibrium points:

$$E_1 = (0,1),\ E_2 = (C-S-1,1),\ E_3 = (0,0),\ E_4 = \left(\frac{k_4\,(C-S)}{k_3+k_4}, \frac{k_3\,(C-S)}{k_3+k_4}\right).$$

We linearize the system of equations (38) to analyze the stability of the equilibria, by using the Hartman–Grobman theorem. The Jacobi matrix for the linearization of the system is

$$J(c,f_b) = \begin{pmatrix} -k_3\,(1-f_b) + k_2\,(C-S-2c-f_b) & k_4 + k_3c - 2k_4f_b - k_2c \\ k_3\,(1-f_b) & -k_4 + 2k_4f_b - k_3c \end{pmatrix}. \tag{41}$$

We shall evaluate the Jacobi matrix at the four equilibrium points and determine the type of the equilibria by the signs of the eigenvalues of the matrix.

1. Equilibrium point $E_1 = (0, 1)$.
   Let us first note that the point E_1 exists only for $C \geq 1$, see Proposition 3. Substituting the latter equilibrium point in (41), we derive:

$$J(E_1) = \begin{pmatrix} k_2\,(C - S - 1) & -k_4 \\ 0 & k_4 \end{pmatrix}.$$

   The eigenvalues of $J(E_1)$ are $\lambda_1 = k_2(C - S - 1)$ and $\lambda_2 = k_4$. Then, obviously, E_1 is a saddle point if $C < S + 1$ holds and an unstable node if $C > S + 1$ is valid.

2. Equilibrium point $E_2 = (C - S - 1, 1)$.
   We substitute E_2 in (41) and obtain

$$J(E_2) = \begin{pmatrix} -k_2\,(C - S - 1) & (C - S - 1)\,(k_3 - k_2) - k_4 \\ 0 & k_4 - k_3\,(C - S - 1) \end{pmatrix}.$$

   The eigenvalues of the triangular matrix are $\lambda_1 = -k_2(C-S-1) < 0$ (from the existence condition) and $\lambda_2 = k_4 - k_3(C-S-1)$. Thus, the equilibrium point is a stable node when $k_4 < k_3(C - S - 1) \iff C > \dfrac{k_4}{k_3} + S + 1$ and is a saddle point when $S + 1 < C < \dfrac{k_4}{k_3} + S + 1$.

3. Equilibrium point $E_3 = (0, 0)$. We compute the determinant and trace of the Jacobi matrix:

$$J(E_3) = \begin{pmatrix} -k_3 + k_2\,(C - S) & k_4 \\ k_3 & -k_4 \end{pmatrix}$$

   and obtain

$$detJ(E_3) = -k_2 k_4\,(C - S)\,, \quad trJ(E_3) = -k_3 - k_4 + k_2(C - S).$$

   The sign of the determinant in this case depends on the factor $C - S$, therefore, we shall consider the following two cases:

   - $C - S > 0$.
     In this case, the determinant is negative and, therefore, E_3 is a saddle point.
   - $C - S < 0$.
     In this case, the determinant is positive and the trace is negative. The equilibrium is, thus, asymptotically stable.

4. Equilibrium point $E_4 = \left(\dfrac{k_4(C-S)}{k_3+k_4}, \dfrac{k_3(C-S)}{k_3+k_4}\right)$.

$$J(E_4) = \begin{pmatrix} -k_3\left(1-\dfrac{k_3(C-S)}{k_3+k_4}\right) - \dfrac{k_2k_4(C-S)}{k_3+k_4} & k_4\left(1-\dfrac{k_3(C-S)}{k_3+k_4}\right) - \dfrac{k_2k_4(C-S)}{k_3+k_4} \\ k_3\left(1-\dfrac{k_3(C-S)}{k_3+k_4}\right) & -k_4\left(1-\dfrac{k_3(C-S)}{k_3+k_4}\right) \end{pmatrix}.$$

For the eigenvalues, after some computations, we obtain

$$\begin{aligned}
\lambda_1\lambda_2 = detJ(E_4) &= \frac{k_2k_4\,(C-S)\,(k_4-k_3(C-S-1))}{k_3+k_4},\\
\lambda_1+\lambda_2 = trJ(E_4)&\\
&= \frac{-k_3(k_3+k_4-k_3(C-S)) - k_2k_4(C-S) - k_4(k_3+k_4-k_3(C-S))}{k_3+k_4}\\
&= \frac{k_3k_4(-1-1+C-S) + k_3^2(-1+C-S) - k_4(k_2(C-S)+k_4)}{k_3+k_4}\\
&= \frac{k_3k_4\,(C-S-2) + k_3^2(C-S-1) - k_4\,(k_2(C-S)+k_4)}{k_3+k_4}.
\end{aligned}$$

In order for the equilibrium point to exist, using Proposition 3, we consider the case when $S < C < S + \dfrac{k_3+k_4}{k_3}$. In this case, the determinant is always positive, therefore, we have to determine the sign of the trace. Further, we shall give an upper bound for the expression of the trace:

$$\begin{aligned}
trJ(E_4) &= \frac{k_3k_4\,(C-S-2) + k_3^2(C-S-1) - k_4\,(k_2(C-S)+k_4)}{k_3+k_4}\\
&= \frac{k_3k_4(C-S-1)}{k_3+k_4} - \frac{k_3k_4}{k_3+k_4} + \frac{k_3^2(C-S-1)}{k_3+k_4} - \frac{k_2k_4(C-S)}{k_3+k_4} - \frac{k_4^2}{k_3+k_4}\\
&< \frac{k_3k_4^2}{k_3(k_3+k_4)} - \frac{k_3k_4}{k_3+k_4} + \frac{k_3^2k_4}{k_3(k_3+k_4)} - \frac{k_2k_4(C-S)}{k_3+k_4} - \frac{k_4^2}{k_3+k_4}\\
&= -\frac{k_2k_4(C-S)}{k_3+k_4}.
\end{aligned}$$

The latter expression is always negative for $C > S$—the case, which we are interested in. Therefore, the equilibrium is asymptotically stable. □

Numerical experiments

Here, we shall present several phase portraits, illustrating Proposition 4. For the numerical experiments, we consider the following values for the parameters, taken from Table 5:

$$k_2 = 5.9,\ k_3 = 65,\ k_4 = 45.$$

Let us note that the initial conditions for the system (38) must satisfy conditions (36).

Experiment 1. In this experiment, we shall consider the model parameters $C = 0.8$ and $S = 0.5$. Thus, we consider the case $0 < S < C < 1$. By Proposition 4, in this case $E_1 = (0, 1)$ and $E_2 = (C - S - 1, 1)$ do not exist, $E_3 = (0, 0)$ is a saddle point, and $E_4 = \left(\dfrac{k_4\,(C-S)}{k_3+k_4}, \dfrac{k_3\,(C-S)}{k_3+k_4}\right)$ is a stable equilibrium. The following is confirmed by the numerical results, depicted in Fig 27.

Experiment 2. We consider the case $0 < C < 1 < S$, thus, we choose the model parameters $C = 0.8$ and $S = 4$. By Proposition 4, $E_1 = (0, 1)$, $E_2 = (C - S - 1, 1)$, $E_4 = \left(\dfrac{k_4\,(C-S)}{k_3+k_4}, \dfrac{k_3\,(C-S)}{k_3+k_4}\right)$ do not exist, while $E_3 = (0, 0)$ is a stable equilibrium. The obtained results, shown in Fig. 28, confirm the latter.

Experiment 3. We shall consider model parameters $C = 4$, $S = 6$, thus, the case $1 < C < S$ holds. Following the statement of Proposition 4, equilibrium points $E_2 = (C - S - 1, 1)$ and $E_4 = \left(\dfrac{k_4\,(C-S)}{k_3+k_4}, \dfrac{k_3\,(C-S)}{k_3+k_4}\right)$ do not exist, while $E_1 = (0, 1)$ is a saddle point, and $E_3 = (0, 0)$ is an asymptotically stable equilibrium point. The numerical results, which confirm the statement of Proposition 4, are shown in Fig. 29.

Experiment 4. In the following experiment, we consider the conditions $S < C < S + 1$ and choose the model parameters $C = 5.2$ and $S = 5$. Taking into account Proposition 4, in this case, E_1 and E_3 are saddle points, E_2 does not exist and E_4 is a stable equilibrium. The numerical results, confirm the statement of the latter proposition, see Fig. 30.

Experiment 5. For Experiment 5, we consider the case $S+1 < C < S+\dfrac{k_3+k_4}{k_3}$ and choose model parameters $C = 5.2$ and $S = 4$. Using Proposition 4, $E_1 = (0, 1)$ is an unstable equilibrium, $E_2 = (C - S - 1, 1)$ and $E_3 = (0, 0)$ are saddle points, while $E_4 = \left(\dfrac{k_4\,(C-S)}{k_3+k_4}, \dfrac{k_3\,(C-S)}{k_3+k_4}\right)$ is asymptotically stable. The numerical results in Fig. 31 are in agreement with the analytic results.

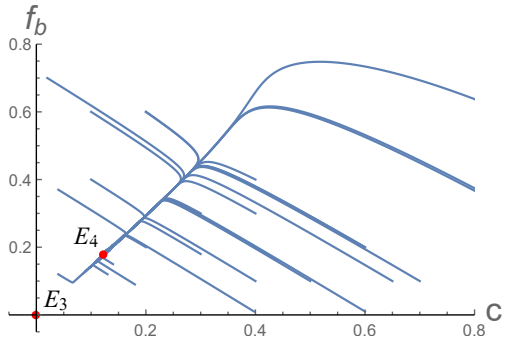

Figure 27: Phase portrait for the case $k_1 = 0$ with parameters $C = 0.8,\ S = 0.5$. E_1 and E_2 do not exist, while E_3 is a saddle and E_4 is a stable equilibrium.

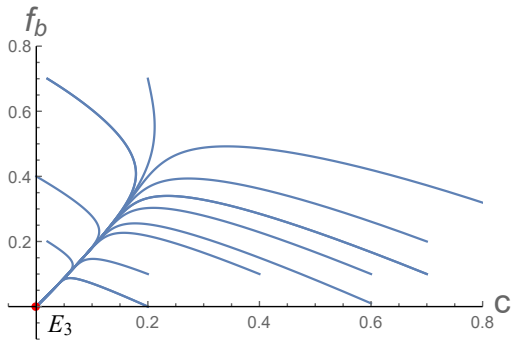

Figure 28: Phase portrait for the case $k_1 = 0$ with parameters $C = 0.8,\ S = 4$. In this case, E_1, E_2, and E_4 do not exist, while E_3 is a stable equilibrium.

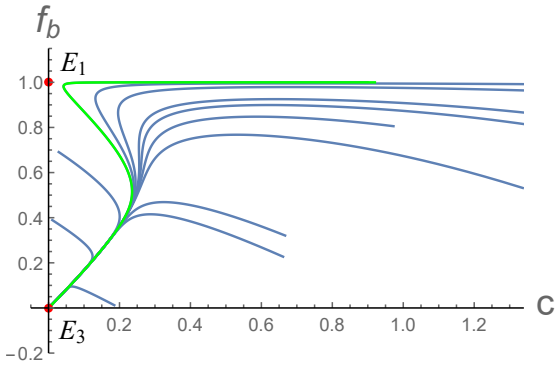

Figure 29: Phase portrait for the case $k_1 = 0$ with parameters $C = 4,\ S = 6$. In this case, E_2 and E_4 do not exist, while E_1 is a saddle and E_3 is an asymptotically stable equilibrium. Note: The green trajectory will be discussed further in the next section.

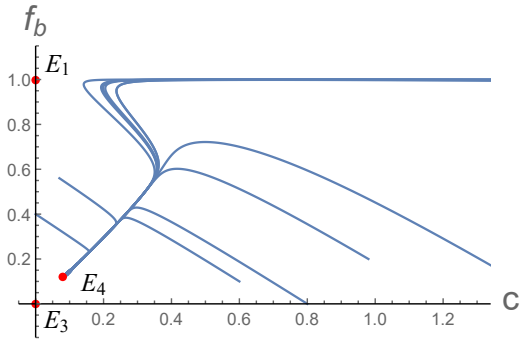

Figure 30: Phase portrait for the case $k_1 = 0$ with parameters $C = 5.2,\ S = 5$. In this case E_1 and E_3 are saddle points, E_2 does not exist, and E_4 is a stable equilibrium.

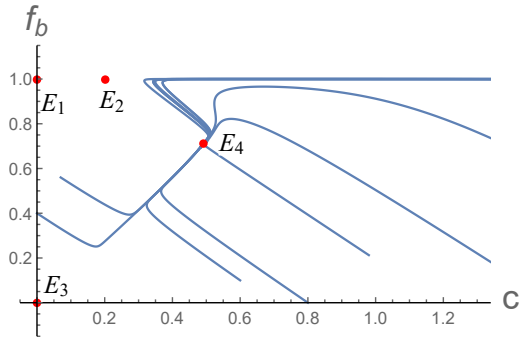

Figure 31: Phase portrait for the case $k_1 = 0$ with parameters $C = 5.2,\ S = 4$. In this case, E_1 is an unstable equilibrium, E_2 and E_3 are saddle points, and E_4 is an asymptotically stable equilibrium.

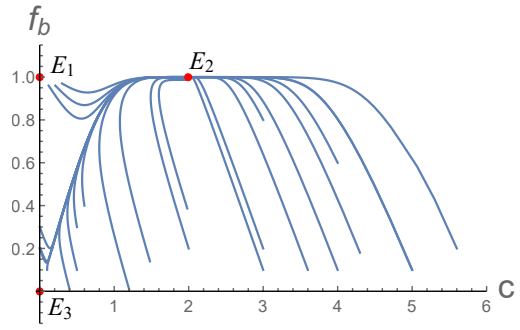

Figure 32: Phase portrait for the case $k_1 = 0$ with parameters $C = 7,\ S = 4$. In this case, E_1 is an unstable equilibrium, E_2 is a stable equilibrium, E_3 is a saddle point, and E_4 does not exist.

Experiment 6. Here, we shall consider the case $C > S + \dfrac{k_3 + k_4}{k_3}$ and choose model parameters $C = 7$, $S = 4$. By Proposition 4, E_1 is an unstable equilibrium, E_2 is asymptotically stable, E_3 is a saddle point and E_4 does not exist. The numerical results in Fig. 32 are in agreement with the analytic results.

3.2.3 Biological implications of the qualitative analysis

Based on the qualitative analysis of the model for the calcium dynamics in a muscle cell, we make the following observations:

- Case $k_1 > 0,\ k_2 = 0$.

  Let us first discuss the case when there is a stimulus, i.e., when $k_2 = 0$. For each choice of the parameters, depending on the ratio C between the total concentrations of calcium ions and CF sites, the biological system tends to a certain equilibrium.

  - Following Proposition 2, when $C < 1$ holds, i.e., when the total concentration of CF sites is more than the total concentration of calcium (or, stated otherwise, there is not enough calcium to fill the CF sites), the system always reaches the equilibrium point $E_2 = \left(\dfrac{Ck_4}{k_3 + k_4}, \dfrac{Ck_3}{k_3 + k_4} \right)$.
  - However, even in the case when there are sufficient calcium ions, depending on the ratio $\dfrac{k_4}{k_3}$ between the rates of binding and release from the CF sites, the system might also stabilize at this point. This is the case, when $C < 1 + \dfrac{k_4}{k_3}$, or equivalently $\dfrac{k_4}{k_3} > C - 1$, thus, the rate of binding of calcium ions to the CF is relatively small, compared to the rate of release;
  - Vice versa, if $\dfrac{k_4}{k_3} < C - 1$, then calcium ions eventually bind to all CF sites, which corresponds to the stable equilibrium $E_1 = (C - 1, 1)$, where $f_b = 1$.

  Let us further note that the equilibrium state of the system does not depend on the rate of release from the SR sites k_1. Therefore, the asymptotic behaviour of the system does not depend on the strength of the incoming signal. However, it determines the rate at which the biological system tends to the equilibrium point. For the sake of example, numerical results for the concentration of free calcium ions, obtained for two different values of k_1, are shown in Fig. 33.

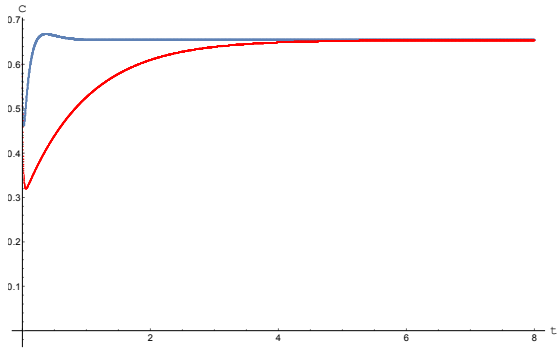

Figure 33: Concentration of free calcium ions c in time. Results for $k_1 = 1$ are depicted in red, for $k_1 = 9.6$—in blue.

- Case $k_1 = 0,\ k_2 > 0$.

  Here, we shall discuss from a biological point of view the qualitative results for the case, when there is no stimulus present in the muscle cell, i.e., when $k_1 = 0$.

  - Following Proposition 4, if $0 < C < S$ holds true, which biologically means that the total concentration of calcium ions is less than the total concentration of SR sites, then the system reaches the equilibrium state $c = 0,\ f_b = 0$. The latter means that all calcium ions get bound to the SR, thus, the muscle cell is relaxed. Let us emphasize that the case $0 < C < S$ is the natural one for the process, since the free calcium ions were originally released from the SR.
  - If, however, the total concentration C is higher than S, then different equilibrium points are reached.

We have discussed in this section the two limiting cases when k_1 and k_2 are held constant, one of them 0. Of course, in reality the process is characterized with consecutive changes in their values. Therefore, the results, presented here, will give us information for the two separate parts of the process—when the stimulus is on and off.

3.3 Numerical experiments

In this section, we shall present only one numerical result to illustrate the process of calcium dynamics, described by model equations (35). More numerical results will be given in the next section, where we shall couple the models for the processes of nerve impulse propagation and calcium dynamics. Here, for model parameters we shall use values from [30], systematized in Table 5.

Parameter	Value	Parameter	Value
C	2	μ_s	600 mN/mm
S	6	l_{s0}	0.234 mm
k_{10}	9.6 s^{-1}	l_{c0}	2.6 mm
k_{20}	5.9 s^{-1}	a	-2.23 mm^{-2}
k_3	65 s^{-1}	α_{max}	1.8
k_4	45 s^{-1}	α_m	0.4 s/mm
L	2.7 mm	α_p	1.33 s/mm
P_0	60.86 mN/mm^2		

Table 5: Model parameters for (35), taken from [30].

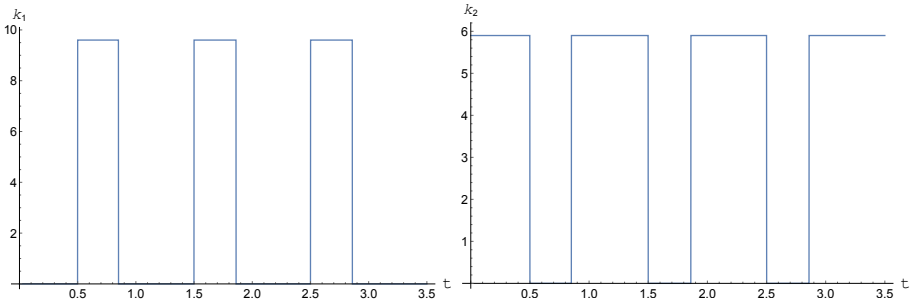

(a) $k_1(t)$ (b) $k_2(t)$

Figure 34: Graphs of coefficients k_1 and k_2.

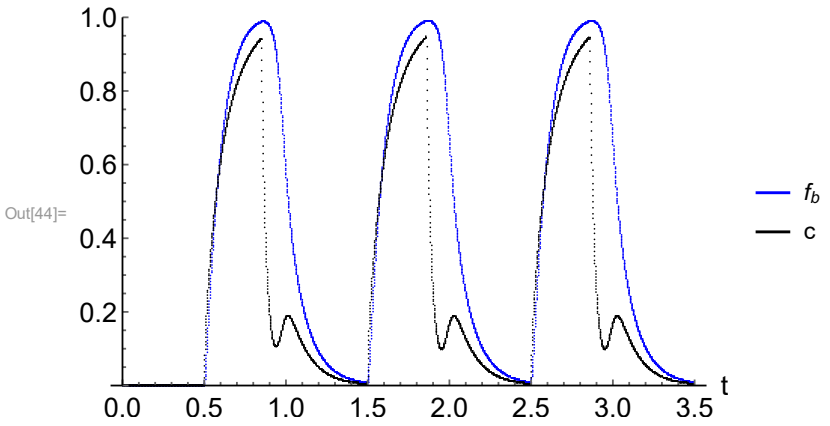

Figure 35: Modelling of calcium dynamics—concentration of free calcium ions (in black), concentration of filament-bound calcium sites (in blue).

Further, we define a square wave stimulus by introducing the piecewise constant functions k_1 and k_2 in the following way:

$$k_1 = \begin{cases} k_{10}, & \text{stimulus is on,} \\ 0, & \text{stimulus is off,} \end{cases} \qquad k_2 = \begin{cases} 0, & \text{stimulus is on,} \\ k_{20}, & \text{stimulus is off.} \end{cases}$$

For our numerical experiment, we consider the particular choice of k_1 and k_2, depicted in Fig. 34.

We solve the system of ODEs in the time domain $t \in [0, 3.5]$, by using the fourth order Runge–Kutta method with the following Butcher table [31]:

0				
1/2	1/2			
1/2	0	1/2		
1	0	0	1	
	1/6	1/3	1/3	1/6

The time-discretization step for the numerical experiments is chosen to be $\Delta t = 10^{-3}$. The numerical solutions for the concentrations c and f_b are shown in Fig. 35.

To explain the numerical results, let us consider the two distinct situations in the process—when the stimulus is on and off.

- Presence of stimulus

  Let us first note that in the case, when $k_2 = 0$, this choice of parameters corresponds to the case of an asymptotically stable point $E_1 = (C - 1, 1)$ in Proposition 2. Thus, for $C = 2$ and $S = 6$, the solution would "try to reach" the corresponding equilibrium point $E_1 = (1, 1)$. The latter is clearly seen from the numerical experiments in Fig. 35.

- Absence of stimulus

  In the case, when the stimulus is off, or equivalently, when $k_1 = 0$, by the qualitative analysis, summarized in Proposition 4, there exist the saddle equilibrium point $E_1 = (0, 1)$ and the asymptotically stable $E_3 = (0, 0)$. The latter explains the peculiar behaviour of the solution for c, that is observed, e.g., around $t = 1$. In particular, let us consider the green trajectory in Fig. 29, which is obtained for an initial condition corresponding to the peak of the graphs in Fig. 4. When close to the saddle point, the trajectory is repelled with a change in the sign of the derivative for the concentration c, which results in rise of the solution for c, followed by a decrease to the equilibrium $c = 0$.

3.4 Conclusion and discussion

In this section, we have considered a mathematical model, described in terms of ordinary differential equations, for the process of calcium dynamics inside the muscle cell. We have obtained results for the qualitative behaviour of the model solutions in the two limiting cases $k_1 = 0$ and $k_2 = 0$ that to the best of our knowledge are not known in the scientific literature. On one hand, such kind of qualitative information is useful in the mathematical modelling of biological processes and it helps to better understand the dynamical properties of the mathematical model. On the other hand, it gives valuable information about the influence of the different model parameters. The latter is particularly interesting, when considering the process in different conditions, e.g., when there are certain diseases present, which affect the normal calcium activity inside the muscle cell.

We have shown that in each case there exists a single (locally) asymptotically stable equilibrium point of the dynamical system. However, the numerical experiments suggest that the corresponding point is also a global attractor for the model solution. It is interesting from a mathematical point of view to establish this result rigorously, which is a question that we shall consider in our further studies on the subject.

Further, it is worth noticing that the model captures only the most significant aspects of the calcium dynamics, related to the calcium release from the SR and its binding to the CFs. However, the whole process of muscle contraction has more details, as discussed in Section 1.2. These could also be considered, in order to construct a more detailed model of the process. In particular, the ATF dynamics is also interesting, e.g., for the process of muscle fatigue.

Also, reaction-diffusion type models could be considered (see, e.g., [32]).

4 Mathematical modelling of neurotransmitter transport in the neuromuscular junction. Integration of the processes.

As discussed in the biological preliminaries in the Introduction, see Section 1.2, once the nerve impulse reaches the axon terminals, neurotransmitters are diffused through the neuromuscular junction to bind to receptors on the muscle cell, thus, causing complex processes in it, resulting in contraction. In the previous sections, we considered two separate models for the processes of nerve impulse transmission and calcium dynamics in the muscle cell, respectively. In the present section, we shall propose two approaches for connecting the model (26), (28) with (35) in one integrated multiphysics model.

As discussed in the previous section, the presence of a signal in the muscle cell is modelled by the coefficients k_1, k_2 in (35). **We shall couple the models**

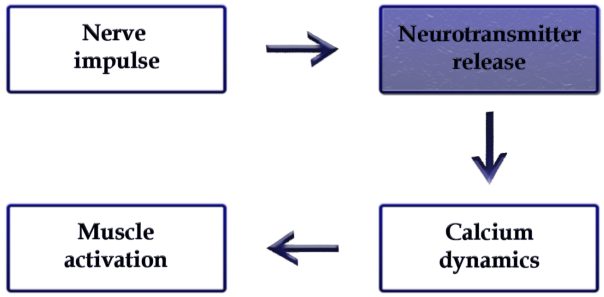

of neural impulse propagation and calcium dynamics by relating k_1 to the result from a numerical simulation of a nerve impulse.

4.1 A simple relation

The first approach we consider in order to get some basic intuition how to connect the models is a rather simplistic one. A direct connection between the nerve impulse and the resulting calcium dynamics is postulated. Let us consider again (35) with the assumptions, proposed by Williams in [29]. In particular, for the coefficients k_1 and k_2, these are:

- when the stimulus is on, $k_1 > 0$ and $k_2 = 0$;
- when the stimulus is off, $k_1 = 0$ and $k_2 > 0$.

We shall assume that **$\mathbf{k_1}$ is proportional to the voltage at the end of the axon**, i.e., at the right boundary of the computational domain.

Let us consider again the numerical results in Section 2.3.2 for a myelinated axon. We shall give two examples—for the single and the periodic stimuli, computed in Experiments 1 and 2, respectively, and depicted in Fig. 36.

The graphs of the corresponding coefficient k_1 that we choose for illustrative purposes are shown in Fig. 37. Let us note that when the voltage is negative, k_1 is set to 0.

Having defined k_1, we proceed in the same way as in the previous section to simulate the calcium dynamics, by solving (35) numerically. Results are depicted in Fig. 38.

The latter results are qualitatively similar to the corresponding ones in Section 3. Here, we shall not go into a greater detail. In this section, we only give a brief idea of our approach for connecting the processes of nerve impulse propagation and calcium dynamics in the muscle cell. In the next section, we shall discuss the biochemical processes that underlie this connection and shall give additional experiments.

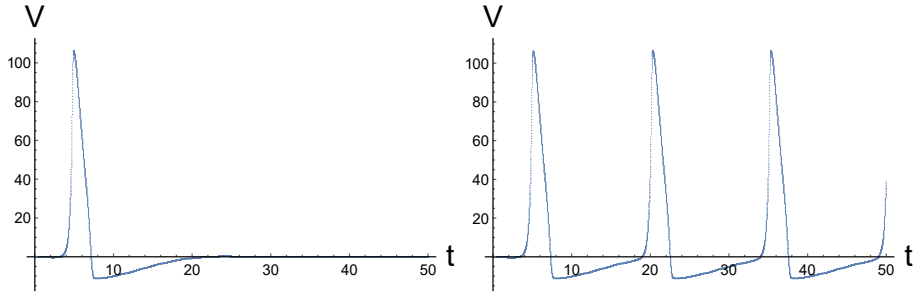

(a) Single impulse (b) Periodic impulse

Figure 36: Graphs of the voltage at the right boundary of an axon.

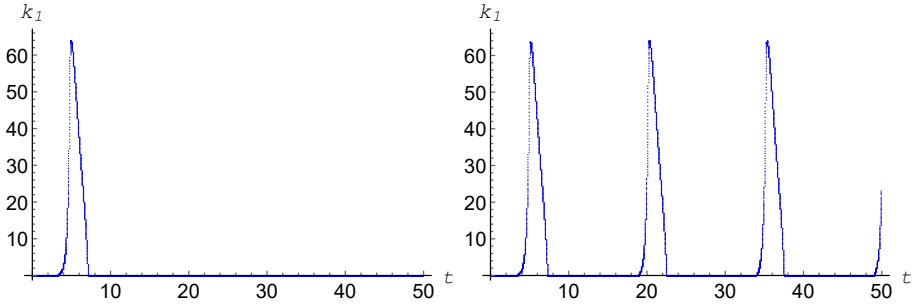

(a) Single impulse (b) Periodic impulse

Figure 37: Graphs of the coefficient k_1, which is chosen proportional to the voltage in Fig. 36, for a single and periodic impulse, respectively.

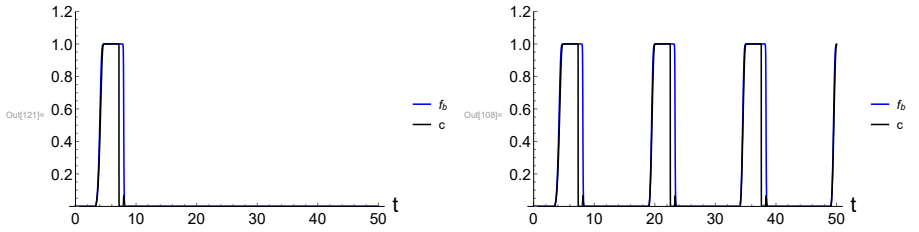

(a) Single impulse (b) Periodic impulse

Figure 38: Numerical solutions for c and f_b, corresponding to k_1 in Fig. 37.

4.2 A reaction–diffusion model of acetylcholine transport in the neuromuscular junction

Now, instead of assuming a simple proportionality between the nerve impulse and the coefficient k_1 in the model of the calcium dynamics, we shall consider a more detailed description of the chemical processes in the neuromuscular junction that result from the neurotransmitter release. As can be seen from Fig. 39, the neuromuscular junction consists of a pre-synaptic membrane (part of the neuron), a post-synaptic membrane (part of the muscle cell), and a synaptic cleft between them.

When an action potential reaches the end of the axon, a neurotransmitter called acetylcholine (ACh) is released in the synaptic cleft. It diffuses to the post-synaptic membrane, where it binds to special receptors (R). In the process, the ACh reacts with the enzyme acetylcholinesterase (AChE), which catalyzes the breakdown of ACh into choline and acetate. Further, on the post-synaptic membrane, when doubly bound with ACh, the receptors open, allowing for the impulse to "go into" the muscle cell. The process can be described by the following reaction schemes (see, e.g., [33], [34], and [35] and the references therein):

$$ACh + R \underset{k_{-r}}{\overset{2k_r}{\rightleftharpoons}} R_1, \quad ACh + R_1 \underset{2k_{-r}}{\overset{k_r}{\rightleftharpoons}} R_2, \quad R_2 \underset{k_c}{\overset{k_o}{\rightleftharpoons}} R_o, \tag{42}$$

where R and R_1 denote the free and single-bound receptors, R_2 denotes the double bound closed ACh receptors, and R_o denotes the open ACh receptors.

The reaction of ACh with AChE can be described by the following reaction scheme:

$$ACh + AChE \underset{k_{-1}}{\overset{k_1}{\rightleftharpoons}} X_1 \xrightarrow{k_2} X_2 + Ch, \quad X_2 \xrightarrow{k_3} AChE + acetate, \tag{43}$$

where X_1 and X_2 denote AChE complexed with ACh and acetyl group, respectively. Choline (Ch) and acetate are end products of the reactions and will not be considered further in the models.

4.2.1 Mathematical formulation

For the model, we assume that the synaptic gap has a cylindrical shape, as shown in Fig. 40. Moreover, we assume that the process is characterized by axial symmetry and in each cross section, the concentrations vary little, thus, we consider a 1D model, where the spatial variable z is defined on the right in Fig. 40.

Let us denote the following:

- a—concentration of ACh;

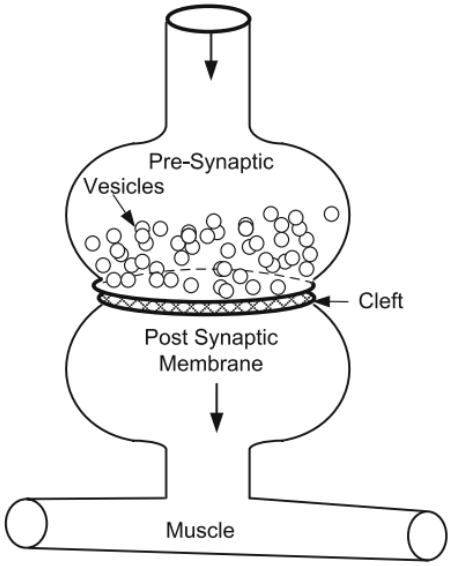

Figure 39: The neuromuscular junction [34].

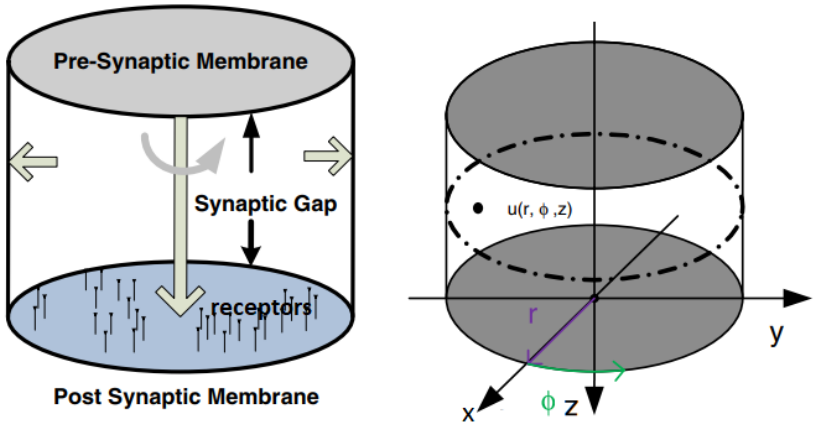

Figure 40: A 3D representation of the neuromuscular junction with its corresponding cylindrical coordinate system [34].

- r_1, r_2, r_o—concentrations of single-bound, double-bound, and opened receptors, respectively;
- x_1, x_2—concentrations of $AChE$ complexes.

By the assumptions we made for the process as well as (42), (43), we consider the following model [35]:

$$\begin{aligned}
\frac{\partial a}{\partial t} &= D\frac{\partial^2 a}{\partial z^2} + F_e(a, x_1, x_2) + \left(F_{r_1}(a, r_o, r_1, r_2) + F_{r_2}(a, r_1, r_2)\right)\delta(z - L),\\
\frac{\partial x_1}{\partial t} &= -F_e(a, x_1, x_2) - k_2 x_1,\\
\frac{\partial x_2}{\partial t} &= k_2 x_1 - k_3 x_2,\\
\frac{dr_1}{dt} &= F_{r_2}(a\big|_{z=L}, r_1, r_2) - F_{r_1}(a\big|_{z=L}, r_o, r_1, r_2),\\
\frac{dr_2}{dt} &= -F_{r_2}(a\big|_{z=L}, r_1, r_2) - F_{r_o}(r_o, r_2),\\
\frac{dr_o}{dt} &= F_{r_o}(r_o, r_2),
\end{aligned} \tag{44}$$

where

$$\begin{aligned}
F_e(a, x_1, x_2) &= -k_1 a\left(E_T - x_1 - x_2\right) + k_{-1} x_1,\\
F_{r_1}(a, r_o, r_1, r_2) &= -2k_r a\left(R_T - r_1 - r_2 - r_o\right) + k_{-r} r_1,\\
F_{r_2}(a, r_1, r_2) &= -k_r a r_1 + 2k_{-r} r_2,\\
F_{r_o}(r_o, r_2) &= k_o r_2 - k_c r_o,
\end{aligned} \tag{45}$$

and the function δ is defined as

$$\delta(x) := \begin{cases} 1, & x = 0,\\ 0, & x \neq 0. \end{cases}$$

For the parameters, we have used the following notation: D is the diffusion coefficient, R_T and E_T are the total concentrations of receptors and AChE, correspondingly, and ks are the rate constants in the reaction schemes (42) and (43). The concentrations r_1, r_2, and r_o are considered only at the boundary $z = L$, thus, they do not depend on the space variable z and the function δ multiplies the corresponding terms in the first equation. The system (44)–(45) is closed with initial conditions for all state variables and two Neumann boundary conditions for a:

$$\frac{\partial a}{\partial z}(0, t) = -a_{left}(t), \quad \frac{\partial a}{\partial z}(L, t) = 0. \tag{46}$$

4.2.2 Numerical scheme

We construct a finite difference approximation of the model (44). Let us discretize the spatial domain $z \in [0, L]$ by introducing a uniform mesh with a discretization step Δz and let $z_i := i\Delta z$, $i = \overline{0, n}$. Analogously, we discretize the time domain $t \in [0, T]$ with a time discretization step Δt and denote $t_j = j\Delta t$, $j = \overline{0, m}$. Further, we denote the approximate solutions for a, x_1, x_2 at the point (z_i, t_j) with A_i^j, $X_{1,i}^j$, and $X_{2,i}^j$, and the approximate solutions for r_1, r_2, and r_o at the point t_j with R_1^j, R_2^j, and R_o^j, respectively.

To this end, because of the stiffness of the system that could be observed, if one tries using classical explicit schemes, we derive a Crank–Nicolson type scheme for the first equation and semi-implicit approximations for the rest.

Approximation of the main equations

- Approximation of the first equation.

  For $i = \overline{1, n-1}, j = \overline{0, m-1}$, we make the following approximation of the first equation in (44):

$$\begin{aligned}\frac{A_i^{j+1} - A_i^j}{\Delta t} = \frac{D}{2}\left(\frac{A_{i+1}^{j+1} - 2A_i^{j+1} + A_{i-1}^{j+1}}{\Delta z^2} + \frac{A_{i+1}^j - 2A_i^j + A_{i-1}^j}{\Delta z^2}\right) \\ + \frac{1}{2}\left(-k_1 A_i^{j+1}\left(E_T - X_{1,i}^{j+1} - X_{2,i}^{j+1}\right) + k_{-1}X_{1,i}^{j+1}\right) \\ + \frac{1}{2}\left(-k_1 A_i^j\left(E_T - X_{1,i}^j - X_{2,i}^j\right) + k_{-1}X_{1,i}^j\right).\end{aligned} \tag{47}$$

- Approximation of the PDEs for the $AChE$ complexes.

  We consider the second and third equations in (44) together. We use a semi-implicit scheme for their approximation. Basically, this is a backward Euler method, but we have approximated a on the j-th time layer in order to avoid the need of solving non-linear algebraic systems:

$$\begin{aligned}\frac{X_{1,i}^{j+1} - X_{1,i}^j}{\Delta t} &= k_1 A_i^j\left(E_T - X_{1,i}^{j+1} - X_{2,i}^{j+1}\right) - k_{-1}X_{1,i}^{j+1} - k_2 X_{1,i}^{j+1}, \\ \frac{X_{2,i}^{j+1} - X_{2,i}^j}{\Delta t} &= k_2 X_{1,i}^{j+1} - k_3 X_{2,i}^{j+1}.\end{aligned} \tag{48}$$

  Let us further note that (48) with $i = \overline{0, n}$ represents $n+1$ uncoupled systems that need to be solved for each time layer $j = \overline{0, m-1}$.

- Approximation of the ODEs for the ACh receptors.

We construct a semi-implicit numerical approximation for the last three equations in (44) in a similar fashion and obtain

$$\begin{aligned}
\frac{R_1^{j+1}-R_1^j}{\Delta t} &= 2k_r A_n^j \left(R_T - R_1^{j+1} - R_2^{j+1} - R_0^{j+1}\right) \\
&\quad - k_{-r} R_1^{j+1} - k_r A_n^j R_1^{j+1} + 2k_{-r} R_2^{j+1}, \\
\frac{R_2^{j+1}-R_2^j}{\Delta t} &= k_r A_n^j R_1^{j+1} - 2k_{-r} R_2^{j+1} - k_o R_2^{j+1} + k_c R_o^{j+1}, \\
\frac{R_o^{j+1}-R_o^j}{\Delta t} &= k_o R_2^{j+1} - k_c R_o^{j+1}, \quad j = \overline{0, m-1}.
\end{aligned} \tag{49}$$

Approximation of the boundary conditions

- Left boundary condition

  We start with the following approximation, which is constructed in accordance with the way we approximated the main equation (i.e., a Crank–Nicolson scheme):

$$\frac{1}{2\Delta z}\left(A_1^{j+1} - A_0^{j+1} + A_1^j - A_0^j\right) = -a_{left}(t_j + \Delta t/2)$$

  Then, similarly to the previous section, by assuming that the main equation is fulfilled on the left boundary with sufficient accuracy, after straightforward, but rather tedious computations that we omit, we increase the order of approximation and derive

$$\begin{aligned}
&\left(-\frac{1}{2\Delta z} - \frac{\Delta z}{2\Delta t D} - \frac{k_1 \Delta z}{4D}\left(E_T - X_{1,0}^{j+1} - X_{2,0}^{j+1}\right)\right) A_0^{j+1} + \frac{1}{2\Delta z} A_1^{j+1} \\
&\quad = -a_{left}(t_j + \Delta t/2) - \frac{A_1^j - A_0^j}{2\Delta z} - \frac{\Delta z}{2\Delta t D} A_0^j - \frac{\Delta z k_{-1}}{4D} X_{1,0}^{j+1} \\
&\quad - \frac{\Delta z}{4D}\left(-k_1 A_0^j \left(E_T - X_{1,0}^j - X_{2,0}^j\right) + k_{-1} X_{1,0}^j\right).
\end{aligned} \tag{50}$$

- Right boundary condition

  We approximate the right boundary condition as follows:

$$\frac{1}{2\Delta z}\left(A_n^{j+1} - A_{n-1}^{j+1} + A_n^j - A_{n-1}^j\right) = 0.$$

  Analogously, we improve the order of approximation and finally obtain

$$\alpha A_{n-1}^{j+1} + \beta A_n^{j+1} = \gamma, \tag{51}$$

where

$$\alpha = -\frac{1}{2\Delta z},$$
$$\beta = \left\{ \frac{1}{2\Delta z} + \frac{\Delta z}{2\Delta t D} + \frac{\Delta z}{4D} k_1 \left(E_T - X_{1,n}^{j+1} - X_{2,n}^{j+1} \right) \right.$$
$$\left. + \frac{2k_r \Delta z}{4D} \left(R_T - R_1^{j+1} - R_2^{j+1} - R_o^{j+1} \right) + \frac{\Delta z}{4D} k_r R_1^{j+1} \right\},$$
$$\gamma = -\frac{1}{2\Delta z} \left(A_n^j - A_{n-1}^j \right) + \frac{\Delta z}{2\Delta t D} A_n^j + \frac{\Delta z}{4D} \left\{ - k_1 A_n^j \left(E_T - X_{1,n}^j - X_{2,n}^j \right) \right.$$
$$+ k_{-1} X_{1,n}^j + F_{r_1}(A_n^j, R_o^j, R_1^j, R_2^j) + F_{r_2}(A_n^j, R_1^j, R_2^j)$$
$$\left. + k_{-1} X_{1,n}^{j+1} + k_{-r} R_1^{j+1} + 2k_{-r} R_2^{j+1} \right\}.$$

Algorithm

The approximations, derived above, can be combined to form the following numerical scheme. After we begin with zero initial conditions at the time layer $j = 0$, we follow the next steps. At each time layer $j = \overline{0, m-1}$:

1. We solve the system (49) and find R_1^{j+1}, R_2^{j+1}, R_o^{j+1};
2. For each $i = \overline{0, n}$, we solve the system (48) and obtain $X_{1,i}^{j+1}$, $X_{2,i}^{j+1}$;
3. We substitute the results from steps 1 and 2 into (47), (50), (51) and solve the resulting system for A_i^{j+1}, $i = \overline{0, n}$.

4.2.3 Numerical experiments

We are now ready to couple all processes, considered so far, in one multiphysics simulation. We shall proceed as follows:

1. **Simulate a nerve impulse (as an example, we use the results from Section 2.3.2);**
2. **Using the results for the voltage at the right boundary of the computational domain, we compute a_{left} and simulate the neurotransmitter transport by implementing (4.6)–(4.10). Note: when the voltage is negative, $a_{\text{left}} = 0$;**
3. **We use the results for R_o from 2 and solve (3.6) with k_1, proportional to R_o, to simulate the calcium dynamics.**

Parameter	Value	Parameter	Value
k_r	30 $\text{mM}^{-1}\text{ms}^{-1}$	k_2	110 ms^{-1}
k_{-r}	10 ms^{-1}	k_3	20 ms^{-1}
k_o	20 ms^{-1}	R_T	2 mM
k_c	5 ms^{-1}	E_T	74 μM
k_1	200 $\text{mM}^{-1}\text{ms}^{-1}$	D	2×10^{-6} cm^2s^{-1}
k_{-1}	1 ms^{-1}	L	50 nm

Table 6: Model parameters for (44), taken from [35].

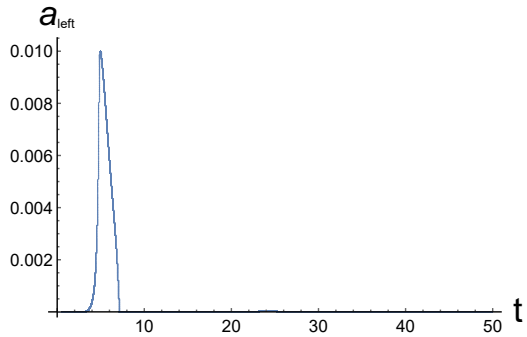

Figure 41: Graph of a_{left} for a single impulse in a myelinated axon.

For our numerical experiments, we consider the parameters in Table 6. The discretization steps for all experiments are chosen to be $\Delta z = 0.5$ and $\Delta t = 0.001$.

Let us note that our main goal of those experiments is to obtain some qualitative results in order to illustrate the main approach. The coefficients of proportionality that we use to couple the models in steps 1–3, certainly, need to be estimated in future studies on the basis of experimental data.

Experiment 1 (Single stimulus input)**.**
For our numerical experiments, we shall follow steps 1, 2, 3 to obtain a multiphysics simulation in the case of a single neural stimulus.

1. We consider the voltage at the right boundary for a myelinated axon, obtained in Section 2.3.2, presented in Fig. 36(a).

2. We choose a_{left} to be proportional to the voltage in 1. The graph of the thus defined a_{left} is shown in Fig. 41.

   The numerical results for a and R_o are depicted in Fig. 42 and Fig. 43, respectively. As evident from the latter, when a nerve impulse is received,

the concentration a rises at the left boundary and starts diffusing through the synaptic cleft. After the axon gets repolarized, the ACh decreases, because it is broken down by the AChE. For our further study, we shall be interested in R_o, in particular. The concentration of the opened receptors will be used to determine the input k_1 in the muscle cell that triggers the calcium dynamics.

3. Last, we choose k_1 for the model (35) to be proportional to the values of R_o, depicted in Fig. 43. The numerical results for the concentrations c and f_b from solving (35) are shown in Fig. 44.

Experiment 2 (Periodic stimulus input)**.**

1. We consider the voltage at the right boundary for a myelinated axon, obtained in Section 2.3.2 presented in Fig. 36(b).

2. We choose a_{left} to be proportional to the voltage in 1. The graph of the thus defined a_{left} is shown in Fig. 45.

   Because we are interested in coupling the process of nerve impulse propagation and calcium dynamics by using the obtained results for R_o, we shall only visualize its concentration, see Fig. 46.

3. We set k_1 for the model (35) to be proportional to the concentration R_o, obtained in 2. The corresponding numerical results are shown in Fig. 47

   The numerical results, obtained in this section, are qualitatively similar to the ones in 3.3. Their advantage, however, is that they are based on a detailed description of the underlying processes.

4.3 Conclusion and discussion

In this section, we have implemented the goal of constructing an example integrated model for the process of muscle activation. We have coupled the processes of nerve impulse propagation, neurotransmitter release and calcium dynamics in the muscle cell. The qualitative behavior of the numerical solutions seems plausible from a biological point of view. In our numerical experiments, we have succeeded in restoring the sequence of events that lead to a muscle contraction—when a nerve impulse is transmitted to the neuromuscular junction, the neurotransmitter acetylcholine is released and diffused to the motor end plate; there, the receptor channels open and lead to calcium dynamics inside the cell.

Let us again note that at this point the obtained results are of qualitative nature. In future work, the parameters that are used for coupling the models should be experimentally identified. Furthermore, the muscle activation is triggered by a whole population of neural cells (cf. [36] and the references therein).

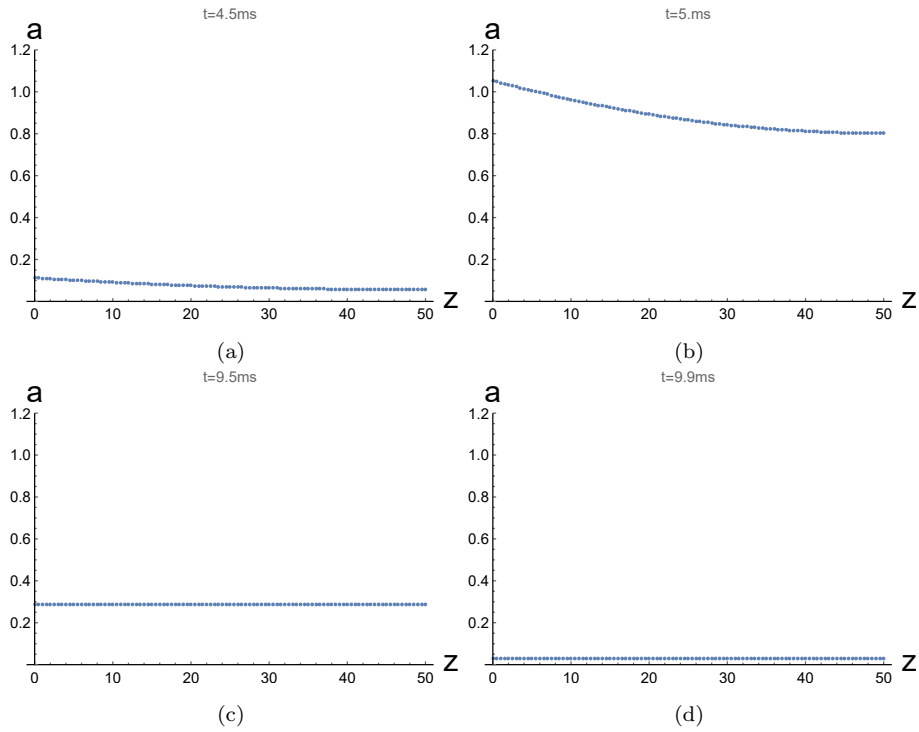

Figure 42: Experiment 1: Time evolution of the ACh concentration.

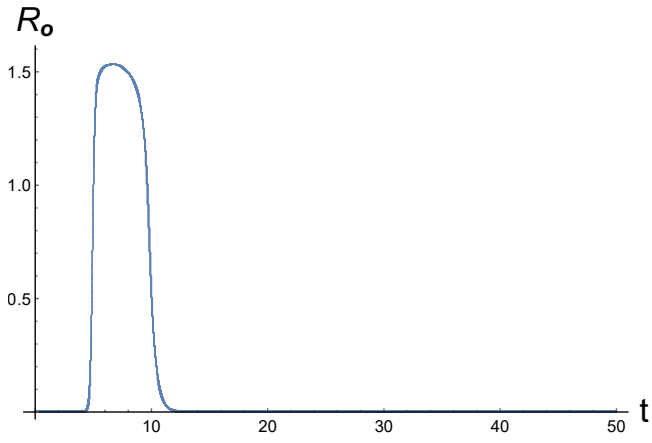

Figure 43: Experiment 1: Time evolution of the concentration R_o of open receptors in the muscle cell membrane.

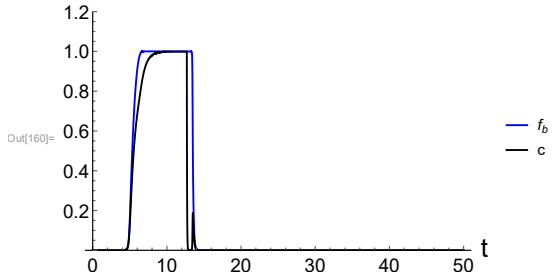

Figure 44: Experiment 2: Graph of the coefficient k_1, which is chosen proportional to the concentration R_o.

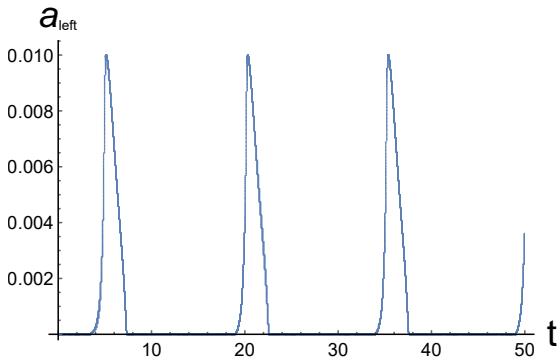

Figure 45: Experiment 2: Graph of a_{left} for a periodic impulse in a myelinated axon.

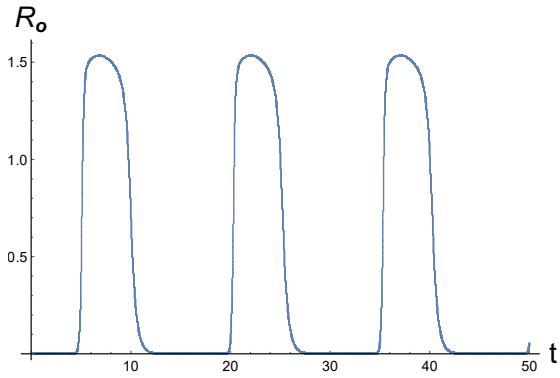

Figure 46: Experiment 2: Time evolution of the concentration R_o of open receptors in the muscle cell membrane.

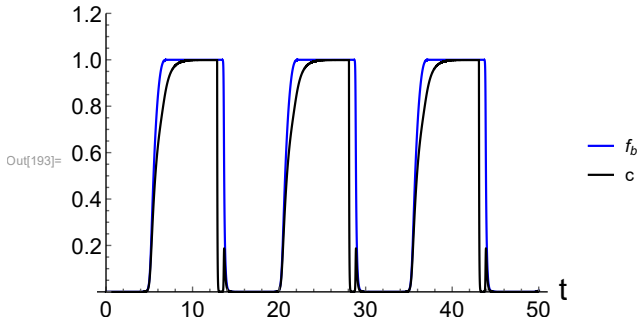

Figure 47: Graph of the concentrations c and f_b, modelled with (35).

Thus, two possible approaches could be undertaken in the future. One can make detailed simulations based on the Hodgkin–Huxley model for a single neuron to compute the effective characteristics for the neural transmission. The other possible approach is to make simulations for some artificial population of neural cells, connected to a muscle cell. In our future work, we plan to study the viability of both approaches.

Another point we should make is that we neglected the radial diffusion in the model of neurotransmitter transport. However, it might be important for the process [35]. Therefore, 2D (axially-symmetric) and 3D models should be considered in our future work.

5 Mathematical modelling of muscle activation

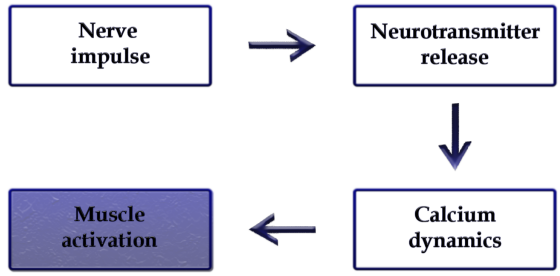

5.1 Mathematical modelling of muscle contraction

In 1938, A. Hill [37] presented the first widely known model of a skeletal muscle. According to Hill, a muscle can be modelled as a contractile element (CE) connected in series with a linearly elastic spring element or series element

(SE) [38], see Fig. 48. The CE generates force due to a signal, resulting from the release of Ca^{2+} ions from the SR, while the elastic spring element has a passive role, which accounts for the tendons. We assume that the total length

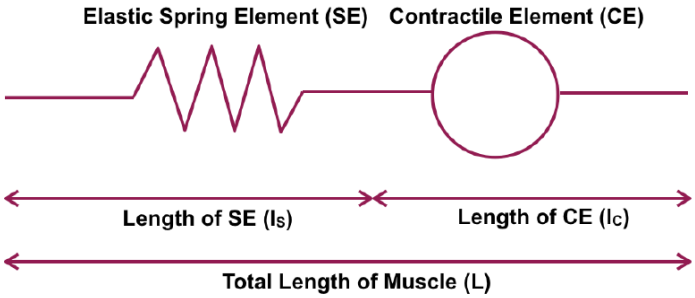

Figure 48: Hill's 1938 model of a muscle [37].

of the muscle L is equal to the sum of the length of the elastic spring element l_s and the length of the contractile element l_c, i.e.,

$$L(t) = l_c(t) + l_s(t). \tag{52}$$

To describe the force in the spring element, we shall use Hooke's law of springs, which states that

$$P_s(t) = \mu_s(l_s(t) - l_{s,0}),$$

where P_s is the force exerted by the spring element, μ_s is the stiffness coefficient, and $l_{s,0}$ is the resting length of the elasting spring element. We express l_s from the above equation and obtain

$$l_s(t) = l_{s,0} + P_s(t)/\mu_s.$$

Substituting the latter in eq. (52), we derive

$$l_c(t) = L(t) - l_{s,0} - P_s(t)/\mu_s. \tag{53}$$

We differentiate (53) and derive the following equation for the velocity of the CE:

$$v_c(t) = V(t) - \frac{1}{\mu_s}\frac{dP_s}{dt}, \tag{54}$$

where v_c and V are the CE and muscle velocities, respectively. For simplicity, we assume an isometric contraction, in which tension is generated without changing the length of the muscle L, i.e., $V(t) \equiv 0$.
The force generation of CE, P_c, depends on the velocity v_c of the element and its length l_c, see [30], thus, as the contraction of the filaments depends on

the binding of Ca^{2+} ions to the CF, P_c is also dependent on the amount of the calcium-bound CF sites, f_b. The latter observations are included in the following possible model:

$$P_c = P_0 \lambda(l_c) g(v_c) f_b, \tag{55}$$

where P_0 is the force, exerted in an isometric tetanic contraction at the resting length $l_{c,0}$ and $g(v_c)$, $\lambda(l_c)$ are used to express the dependence of P_c on the length l_c and the velocity v_c. The latter functions $\lambda(l_c)$ and $g(v_c)$ are estimated from the measurements in Williams, et.al. [29], where experiments were performed on a lamprey muscle. Positive velocity v_c is assumed to refer to lengthening of the CE, while a negative one means shortening. Further, $g(v_c)$ is assumed to be a piecewise linear function:

$$g(v_c) = 1 + \begin{cases} \alpha_p v_c, & v_c \geq 0, \\ \alpha_m v_c, & v_c < 0, \end{cases} \tag{56}$$

where $\alpha_p > \alpha_m > 0$, because of the ability of muscle fibers to exert greater forces during lengthening than shortening [29] and $0 \leq g(v_c) \leq \alpha_{max}$.
The equation that defines $\lambda(l_c)$, according to Williams [29], is given by

$$\lambda(l_c) = 1 + a(l_c - l_{c,0})^2. \tag{57}$$

The above function has a minimum, equal to 1, at the equilibrium length.

Since the CE and SE are connected in series, P_c and P_s should be equal in a steady state. If we set $P_c = P_s$, then we can reduce (54) and (55) to one expression for v_c, dependent on the derivatives of the functions in (56) and (57). The piecewise function g, however, is not differentiable at $v_c = 0$, which will result in singularity in the obtained equation [9]. Furthermore, the stretch of the SE in reality is not instantaneous [30]. Therefore, this approach is not used, but a simple linear kinetics is considered:

$$\frac{dP_s}{dt} = k_5 \left(P_c - P_s\right),$$

where k_5 is chosen large enough so that P_s and P_c are nearly identical.

We substitute (55) in the latter equation:

$$\frac{dP_s}{dt} = k_5 \left(P_0 \lambda(l_c)(1 + \alpha v_c) f_b - P_s\right), \quad \alpha = \begin{cases} \alpha_p, & v_c \geq 0, \\ \alpha_m, & v_c < 0. \end{cases}$$

Then, using (54), we obtain:

$$\frac{dP_s}{dt} = k_5 \left(P_0 \lambda(l_c) \left(1 + \alpha \left(V(t) - \frac{1}{\mu_s} \frac{dP_S}{dt}\right)\right) f_b - P_s\right), \ \alpha = \begin{cases} \alpha_p, & v_c \geq 0, \\ \alpha_m, & v_c < 0. \end{cases}$$

Rearranging the terms, we derive the following equation for P_s:

$$\frac{dP_s}{dt} = k_5\mu_s \frac{P_0\lambda(l_c)f_b\left(1+\alpha V(t)\right) - P_s}{\mu_s + k_5P_0\lambda(l_c)\alpha f_b}, \quad \alpha = \begin{cases} \alpha_p, & v_c \geq 0, \\ \alpha_m, & v_c < 0. \end{cases} \tag{58}$$

5.2 Numerical experiments

In this section, we show how one can use Hill's model to simulate nerve force generation by using f_b from (35) as an input to (58). For our numerical experiments, we consider the parameters given in Table 5. We substitute the assumption of $V(t) = 0$ in (58) and derive

$$\frac{dP_s}{dt} = k_5\mu_s \frac{P_0\lambda(l_c)f_b - P_s}{\mu_s + k_5P_0\lambda(l_c)\alpha f_b}. \tag{59}$$

We further express l_c from (53) and substitute in (57), thus, consider the function λ as a function of the spring force P_s, $\lambda(P_s)$:

$$\lambda(P_s) = 1 + a\left(L - l_{s0} - \frac{P_s}{\mu_s} - l_{c,0}\right)^2. \tag{60}$$

Substituting the latter in (59), we derive

$$\frac{dP_s}{dt} = k_5\mu_s \frac{P_0\lambda(P_s)f_b - P_s}{\mu_s + k_5P_0\lambda(P_s)\alpha f_b}. \tag{61}$$

We discretize the time domain $t \in [0, T]$, by introducing a uniform mesh

$$\omega_{\Delta t} := \{t_i = i\Delta t,\ i = \overline{0, n},\ n = T/\Delta t\}$$

and denote $\bar{P}_{s,i}$ and $\bar{v}_{c,i}$ to be the values of the approximate solution at t_i. We further approximate the time derivative in (61), using forward difference formula. In order to estimate v_c (which is used to obtain α), we use use backward difference formula. Thus, we make the computations, using the following numerical scheme:

$$\begin{aligned} &\frac{\bar{P}_{s,i+1} - \bar{P}_{s,i}}{\Delta t} = k_5\mu_s \frac{P_0\lambda(\bar{P}_{s,i})f_{b,i} - \bar{P}_{s,i}}{\mu_s + k_5P_0\lambda(\bar{P}_{s,i})\alpha f_{b,i}}, && i = \overline{0, n-1}, \\ &\bar{v}_{c,i} = \frac{\bar{P}_{s,i-1} - \bar{P}_{s,i}}{\Delta t\mu_s}, && i = \overline{1, n}, \\ &\bar{P}_{s,0} = 0, \quad \bar{v}_{c,0} = 0. \end{aligned}$$

The numerical results, corresponding to $\Delta t = 0.001$, are presented in Fig. 49, where the values of $f_{b,i}$ are taken from the computations in Section 3.3.

The results in Fig. 35 and Fig. 49 show that when k_1 is positive, i.e., when the stimulus is on, the concentration of free calcium ions and calcium-bound CF sites increases as well as the generated force. On the other hand, when k_1 is zero and $k_2 > 0$ (i.e., the stimulus is off), the three quantities decrease.

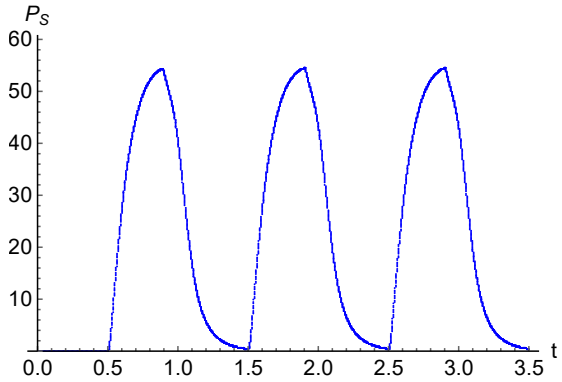

Figure 49: Resulting muscle force, simulated with Hill's model [37].

5.3 Conclusion and discussion

As we can see, it is straightforward to compute the resulting muscle force, using Hill's model, if we have simulated the calcium dynamics inside the muscle cells. We have shown only an experiment, corresponding to the results in Section 3. Numerical simulations for the integrated approach presented in the previous section can be obtained in the same way.

In the literature, there exist other models for the muscle force generation. Another classical one, besides Hill's model, is Huxley's model, see [39]. Such models could also be considered in our future work.

6 Conclusion

The neuromuscular system combines the nervous system and muscles together to control and permit movement of the body. The process of muscle activation can be described by four consecutive subprocesses—nerve impulse propagation, neurotransmitter release in the neuromuscular junction, calcium dynamics in the muscle cell, and muscle force generation. A disorder in one of the latter processes is known as a neuromuscular disease. Thus, the neuromuscular diseases could be divided in the following groups [40]:

- motor neuron diseases;
- neuromuscular junction disorders;
- muscle diseases.

Studying each of the latter necessitates an in-depth study of the underlying mechanisms of neuromuscular activation and the effect of the specific disorder to the whole process.

In this thesis, we have described in details the process of muscle activation and have derived a mathematical model for each of the related subprocesses. Further, we have proposed a framework, which couples the latter models. The results from studying these models and possible directions for future studies were summarized in each individual section and we shall not repeat the conclusions here.

Let us note, however, the following. The aim of the framework is to allow separate modelling of the processes as well as obtaining an integrated simulation for the muscle activity. We plan to use this framework as a cornerstone for our future studies of neuromuscular diseases. The framework can be adapted for specific purposes by modifying or substituting the considered mathematical models as well as adding additional processes. Also, a comparison with other known in the literature integrated models (see, e.g., [41], [42] and the references therein) should be made from the point of view of their applicability to studying neuromuscular diseases.

A Additional information, concerning the Hodgkin–Huxley model

A.1 Basic physical laws, used in the derivation of the Hodgkin–Huxley model

A.1.1 Charge conservation law

Let us denote the transmembrane voltage and the electric charge at position x and time t by $V(x,t)$ and $q(x,t)$, respectively, the total current with $j(x,t)$ and the longitudinal current with $i(x,t)$. We consider a small interval $[\xi, \xi+\Delta\xi]$, see Fig. 50.

The law of conservation of charge states that the change in the amount of electric charge in a given volume of space is equal to the amount of charge, flowing into the volume minus the amount of charge, flowing out of the volume. Therefore, it gives a relation between the amount of charge and the charge flux in a specific volume. We can write it in mathematical terms as follows:

$$\frac{d}{dt}\int_{\xi}^{\xi+\Delta\xi} q\ dx = \int_{\xi}^{\xi+\Delta\xi} \frac{\partial q}{\partial t}\ dx = i(\xi,t) - i(\xi+\Delta\xi,t). \tag{62}$$

We substitute with the definition of current, i.e., $j = \dfrac{\partial q}{\partial t}$ and approximate the integral on the left-hand side using the midpoint rule [43], to obtain

$$j\left(\xi + \frac{\Delta\xi}{2}, t\right)\Delta\xi = i(\xi,t) - i(\xi+\Delta\xi,t) + O\left((\Delta\xi)^3\right).$$

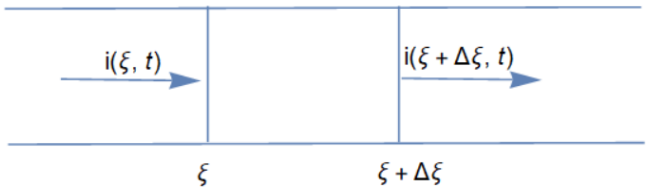

Figure 50: Longitudinal flow of current in the interval $[\xi, \xi + \Delta\xi]$.

Then, we divide both sides by $\Delta\xi$ and let $\Delta\xi \to 0$ to finally derive the **differential form of the conservation law of charge**:

$$j(\xi, t) = -\frac{\partial i}{\partial x}(\xi, t)\,. \tag{63}$$

A.1.2 Ohm's law

Ohm's law states that the current, passing through a conductor, is proportional to the voltage and inversely proportional to the resistance. If a constant resistance R is assumed, then the following holds true:

$$i(x, t) = \frac{V(x, t)}{R}. \tag{64}$$

We shall derive a relation between the charge q and the voltage V. Let us again consider a small interval $[\xi, \xi+\Delta\xi]$. The membrane voltage at point ξ is equal to the difference in the electric potentials inside and outside the axon. Assuming that the potential outside the axon is equally distributed, i.e., a constant, we express the voltage in terms of the inside potential V_{in} and the outside potential V_{out}:

$$\begin{aligned} V(\xi, t) &= V_{in}(\xi, t) - V_{out}, \\ V(\xi + \Delta\xi, t) &= V_{in}(\xi + \Delta\xi, t) - V_{out}. \end{aligned} \tag{65}$$

Subtracting the two equations in (65), we derive:

$$V(\xi, t) - V(\xi + \Delta\xi, t) = V_{in}(\xi, t) - V_{in}(\xi + \Delta\xi, t). \tag{66}$$

The right-hand side is equal to the voltage in the interval $[\xi, \xi + \Delta\xi]$. Taking the latter into consideration and combining (64) for the longitudinal current i with (66), we obtain:

$$\int_{\xi}^{\xi+\Delta\xi} R\; i(x, t)\; dx = V(\xi, t) - V(\xi + \Delta\xi, t).$$

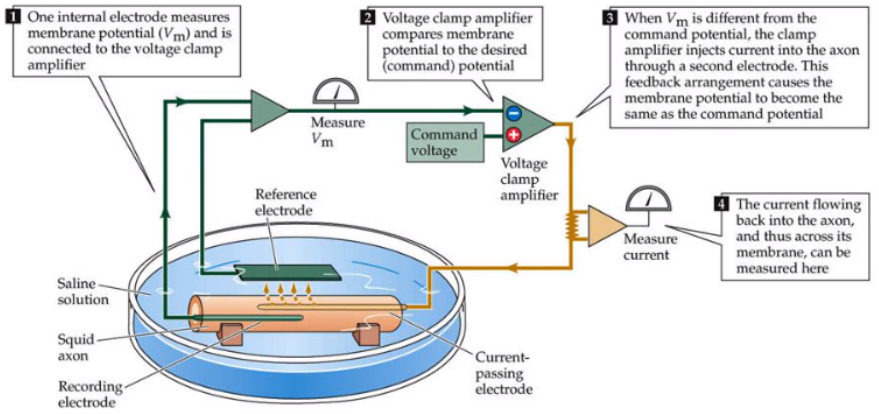

Figure 51: Schematic representation of the voltage clamping technique [44].

We again approximate the integral in the latter equation by using the midpoint rule and obtain:

$$R\, i\left(\xi + \frac{\Delta\xi}{2}, t\right)\Delta\xi = V(\xi, t) - V(\xi + \Delta\xi, t) + O\left((\Delta\xi)^3\right).$$

By taking the limit $\Delta\xi \to 0$, we derive:

$$R\, i(x,t) = -\frac{\partial V}{\partial x}(x,t). \tag{67}$$

A.2 The experiments of Hodgkin and Huxley

A.2.1 Space and voltage clamping

To model the current through the membrane of the axon, Hodgkin and Huxley used the following two techniques to formulate empirical laws for the transmembrane current [13].

- Space clamping
  A squid nerve has a long axon. Because of its length, variations in the transmembrane voltage are expected, which makes it difficult to measure the ionic permeability of the membrane. The idea of space clamping is to eliminate space as an independent variable, i.e., it is held constant in space. For this technique a conducting longitudinal wire is inserted, which results in a uniform potential throughout the length of axon surrounding the wire.

- Voltage clamping
  The idea of voltage clamping is to hold the transmembrane voltage at a fixed value in order to measure other important variables that describe the propagation of an impulse, such as ionic current, membrane permeability, temperature, etc. This is done by using an electronic device called negative-feedback amplifier. A schematic representation of the experimental setup is given in Fig. 51.

A.2.2 Sodium and potassium "turn-on" and "turn-off" variables

To understand in more details the dynamics, described by the Hodgkin–Huxley model, let us consider the sodium and potassium "turn-on" and "turn-off" variables m, n, and h, separately. The latter are modeled by (8)–(10). Considering the model for a fixed V, we obtain the following ODE system:

$$\begin{aligned}\frac{dm}{dt} &= -\frac{m - m_0(V)}{\tau_m(V)},\\ \frac{dh}{dt} &= -\frac{h - h_0(V)}{\tau_h(V)},\\ \frac{dn}{dt} &= -\frac{n - n_0(V)}{\tau_n(V)}.\end{aligned}$$

Example solutions for fixed $V = 100$ mV are shown in Fig. 52.

As can be seen in Fig. 52, the functions $m(t)$, $h(t)$, $n(t)$ tend to equilibrium states—those are $m_0(100)$, $n_0(100)$, $h_0(100)$, respectively. In the initial stage of the process, m changes much faster than h and n do. This is why we can think of m as describing the opening of the sodium channels—since h is close to 1, while m reaches its equilibrium, the dynamics of the product m^3h is determined by m, when t is sufficiently small. After that, m gets stabilized, therefore m^3h tends to zero as h does, i.e., h describes the closing of the sodium channels. Analogously, we can note that the dynamics of the potassium channels is much slower than the opening of the sodium channels.

B Qualitative analysis

Here, we give some basic notions from the qualitative theory of dynamical systems that is used in the thesis. Much more detailed exposition of the subject can be found, e.g., in [45], [46], [47].

We consider an autonomous ODE system

$$\frac{d\mathbf{u}}{dt} = \mathbf{f}(\mathbf{u}), \tag{68}$$

where $\mathbf{u} \in \mathbb{R}^n$ and $\mathbf{f} : \mathbb{R}^n \to \mathbb{R}^n$ is a sufficiently smooth function.

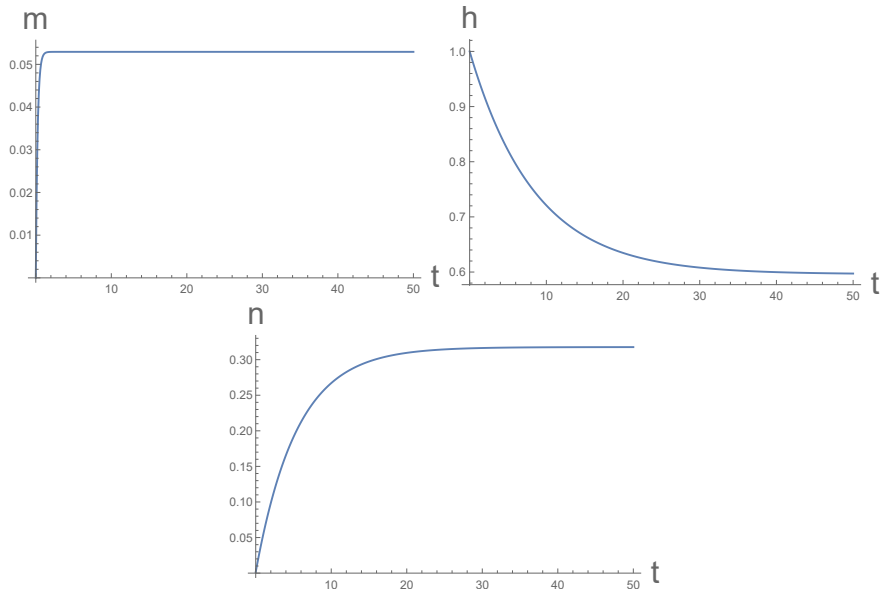

Figure 52: Solutions for the sodium and potassium turn-on and turn-off variables m, h, and n at a fixed voltage of 100 mV.

Definition 1. *The set of all possible values of* $\boldsymbol{u}$ *is called a phase space.*

Definition 2. *The projection of a solution of the system* (68) *onto the phase space is called a trajectory.*

Definition 3. *We say that the equilibrium point* E *is Lyapunov stable, if* $\forall \epsilon > 0$, $\exists \delta = \delta(\epsilon) > 0$ *such that if* $|\mathbf{u}_0 - E| < \delta$ *it follows that* $|\gamma(t) - E| < \epsilon$ *for every* t*, where* $\gamma(t)$ *is the trajectory, corresponding to the initial condition* $\boldsymbol{u}_0$ *from the phase space. If in addition* $\gamma(t) \to E$ *as* $t \to \infty$*, then* E *is called asymptotically stable.*

Definition 4. *We say that the point* E *from the phase space is an equilibrium point of* (68)*, if it is a solution of the system* $\boldsymbol{f}(\boldsymbol{u}) = \mathbf{0}$*.*

Theorem 1 (Hartman–Grobman)**.** *Let* E *be an equilibrium point for the system* (68)*. If* E *is hyperbolic, i.e., if the eigenvalues of the Jacobi matrix* J *of the right-hand side, evaluated at the point* E*, have non-zero real parts, then, in a sufficiently small neighborhood of the point* E*, the dynamics of the linearized system*

$$\frac{d\boldsymbol{u}}{dt} = J(E)(\boldsymbol{u} - E),$$

is the same as the dynamics of the original system.

Let us consider (68) for $n = 2$. From the Hartman–Grobman theorem and known results for linear autonomous systems, it follows that:

- if $\lambda_1 < 0$ and $\lambda_2 < 0$, where λ_1 and λ_2 are the eigenvalues of the Jacobi matrix, the equilibrium point E is asymptotically stable;
- if at least one of the eigenvalues is positive, then E is unstable; in particular, if exactly one of the eigenvalues is negative and the other is positive, then E is a saddle point.

References

[1] Muscular Distrophy Canada, "Types of Neuromuscular Disorders", [07/02/2023].

[2] Wikipedia, "Neuromuscular disease", [07/02/2023].

[3] W. Frontera, J. Ochala, "Skeletal Muscle: A Brief Review of Structure and Function", *Calcified Tissue International volume*, 96:183-195, 2015.

[4] YouTube, "Anatomy of a muscle cell", [07/02/2023].

[5] J. Betts, et.al., "Anatomy and Physiology", OpenStax, Technical report, 2013.

[6] Wikipedia, "Neuron", [07/02/2023].

[7] J. D. Wood, "Chapter 21 – Cellular Neurophysiology of Enteric Neurons", *Physiology of the Gastrointestinal Tract (Fifth Edition)*, 1:629-669, 2012.

[8] Wikipedia, "Chemical synapse", [07/02/2023].

[9] T. Meredith, "A Mathematical Model of the Neuromuscular Junction and Muscle Force Generation in the Pathological Condition Myasthenia Gravis", *Semantic Scholar*, Art. 52036412, 2018.

[10] Wikipedia, "Muscle contraction", [07/02/2023].

[11] M. Dominguez, "Action Potential Conduction", [07/02/2023].

[12] Wikipedia, "Sliding filament theory", [07/02/2023].

[13] A. Scott, *Neuroscience: A Mathematical Primer*, Springer, New York, 2002.

[14] J. Bell, "Behaviour of Some Models of Myelinated Axons", *Mathematical Medicine and Biology: A Journal of the IMA*, 1(2):149-167, 1984.

[15] Quora, "What are neurons made of?", [07/02/2023].

[16] Lumen Learning, "Resting Membrane Potential, [07/02/2023].

[17] Wikipedia, "Ion channel", [07/02/2023].

[18] Wikipedia, “Capacitor”, [07/02/2023].

[19] Khan Academy, “Capacitor article”, [07/02/2023].

[20] Course Hero, “Capacitors and Dielectrics”, [07/02/2023].

[21] Antranik, “What is an Action Potential? (Nerve Impulse)”, [07/02/2023].

[22] M. A. Clark, M. Douglas, J. Choi, “Biology 2e”, OpenStax, 2018.

[23] S. Dimova, T. Chernogorova, A. Yotova, *Numerical Methods for Differential Equations*, Sofia University Publishing House, 2010 (in Bulgarian).

[24] R. Fitzhugh, “Computation of Impulse Initiation and Saltatory Conduction in a Myelinated Nerve Fiber”, *Biophysical Journal*, 2(1):11-21, 1962.

[25] H. Chi, J. Bell, B. Hassard, “Numerical solution of a nonlinear advance-delay-differential equation from nerve conduction theory”, *Journal of Mathematical Biology*, 24:583-601, 1986.

[26] A. Carpio, “Asymptotic construction of pulses in the discrete Hodgkin-Huxley model for myelinated nerves”, *Physical Review E*, 72:011905, 2005.

[27] Wikipedia, “Kirchhoff’s circuit laws”, [07/02/2023].

[28] Z. D. Nedyalkova, T. B. Ivanov, “Qualitative analysis of a mathematical model of calcium dynamics inside the muscle cell”, *Annual of Sofia University “St. Kliment Ohridski”, Faculty of Mathematics and Informatics*, 106:127-151, 2019.

[29] T. Williams, G. Bowtell, N. A. Curtin, “Predicting force generation by lamprey muscle during applied sinusoidal movement using a simple dynamic model”, *Journal of Experimental Biology*, 201(6):869-875, 1998.

[30] T. McMillen, T. Williams, P. Holmes, “Nonlinear Muscles, Passive Viscoelasticity and Body Taper Conspire To Create Neuromechanical Phase Lags in Anguilliform Swimmers”, *PLOS Computational Biology*, 4(8):e1000157, 2008.

[31] J. C. Butcher, *Numerical Methods for Ordinary Differential Equations*, Second Edition, Wiley, 2008.

[32] A. M. Alexander, E. K. DeNardo, E. Frazier III, M. McCauley, N. Rojina, “Spontaneous Calcium Release in Cardiac Myocytes: Store Overload and Electrical Dynamics”, *Spora: A Journal of Biomathematics*, 1(1):36-48, 2015.

[33] A. Friboulet, D. Thomas, “Reaction-diffusion Coupling in a Structured System: Application to the Quantitative Simulation of Endplate Currents”, *Journal of Theoretical Biology*, 160(4):441-455, 1993.

[34] A. Khaliq, F. Jenkins, M. DeCoster, W. Dai, “A new 3D mass diffusion–reaction model in the neuromuscular junction”, *Journal of Computational Neuroscience*, 30:729-745, 2011.

[35] T. Naka, K. Shiba, N. Sakamoto, "A two-dimensional compartment model for the reaction-diffusion system of acetylcholine in the synaptic cleft at the neuromuscular junction", *Biosystems*, 41(1):17-27, 1997.

[36] T. Heidlauf, F. Negro, D. Farina, O. Röhrle, "An integrated model of the neuromuscular system", *2013 6th International IEEE/EMBS Conference on Neural Engineering (NER)*, IEEE, 227-230, 2013.

[37] A. V. Hill, "The heat of shortening and the dynamic constants of muscle", *Proceedings of the Royal Society of London. Series B – Biological Sciences*, 126(843):136-195, 1938.

[38] K. Jovanović, J. Vranic, N. Miljković, "Hill's and Huxley's muscle models – tools for simulations in biomechanics", *Serbian Journal of Electrical Engineering*, 12(1):53-67, 2015.

[39] A. F. Huxley, "Muscle structure and theories of contraction", *Progress in Biophysics and Biophysical Chemistry*, 7:256-319, 1957.

[40] A. Reeves, R. Swenson, *Disorders of the Nervous System: A Primer*, Dartmouth Medical School, 2004.

[41] J. Fernandez, J. Zhang, T. Heidlauf, M. Sartori, T. Besier, O. Röhrle, D. Lloyd, "Multiscale musculoskeletal modelling, data-model fusion and electromyography-informed modelling", *Interface Focus*, 6:20150084, 2016.

[42] M. Sreenivasa, K. Ayusawa, Y. Nakamura, "Modeling and Identification of a Realistic Spiking Neural Network and Musculoskeletal Model of the Human Arm, and an Application to the Stretch Reflex", *IEEE Transactions on Neural Systems and Rehabilitation Engineering*, 24:(5):591-602, 2016.

[43] B. Boyanov, *Lectures in Numerical Methods*, Darba, 1998 (in Bulgarian).

[44] Neuroscience, "The Voltage Clamp Technique", [07/02/2023].

[45] J. K. Hale, *Ordinary Differential Equations*, Wiley, 1980.

[46] Y. Kuznetsov, *Elements of Applied Bifurcation Theory*, Third Edition, Applied Mathematical Sciences, 112, Springer, New York, 2004.

[47] S. Wiggins, *Introduction to Applied Nonlinear Dynamical Systems and Chaos*, Second Edition, Texts in Applied Mathematics, 2, Springer, New York, 2003.